Carbohydrate Polymers 320 (2023) 121214

Contents lists available at ScienceDirect

Carbohydrate Polymers

journal homepage: www.elsevier.com/locate/carbpol

Low-molecular weight sulfated marine polysaccharides: Promising molecules to prevent neurodegeneration in mucopolysaccharidosis IIIA?

Noemi Veraldi [a,*], Isabelle Dentand Quadri [b], Yohan van de Looij [c,d], Laura Malaguti Modernell [d], Corinne Sinquin [e], Agata Zykwinska [e], Benjamin B. Tournier [f], Fabien Dalonneau [g], Honglian Li [h], Jin-Ping Li [h], Philippe Millet [f], Romain Vives [g], Sylvia Colliec-Jouault [e], Ariane de Agostini [a,b], Eduardo Farias Sanches [d], Stéphane V. Sizonenko [d]

[a] Division of Clinical Pathology, Department of Diagnostics, Geneva University Hospitals, Geneva, Switzerland
[b] Department of Pathology and Immunology, Faculty of Medicine, Geneva University, Geneva, Switzerland
[c] Center for Biomedical Imaging, Animal Imaging Technology section, Federal Polytechnic School of Lausanne, Lausanne, Switzerland
[d] Division of Development and Growth, Department of Pediatrics & Gynecology & Obstetrics, Children's Hospital, Geneva University Hospitals, Geneva, Switzerland
[e] Ifremer, Atlantic Center, MASAE, Nantes, France
[f] Division of Adult Psychiatry, Department of Psychiatry, Geneva University Hospitals, Geneva, Switzerland
[g] University of Grenoble Alpes, CNRS, CEA, IBS, Grenoble, France
[h] Department of Medical Biochemistry and Microbiology, Uppsala University, Sweden

ARTICLE INFO

Keywords:
Heparan sulfate
Mucopolysaccharidosis
Marine polysaccharides
Magnetic spectroscopy resonance

ABSTRACT

Mucopolysaccharidosis IIIA is a hereditary disease caused by mutations in the sulfamidase enzyme that participates in catabolism of heparan sulfate (HS), leading to HS fragment accumulation and multisystemic failure. No cure exists and death occurs around the second decade of life. Two low molecular weight highly sulfated compounds derived from marine diabolican and infernan exopolysaccharides (A5_3 and A5_4, respectively) with heparanase inhibiting properties were tested in a MPSIIIA cell line model, resulting in limited degradation of intracellular HS. Next, we observed the effects of intraperitoneal injections of the diabolican derivative A5_3 from 4 to 12 weeks of age on MPSIIIA mice. Brain metabolism and microstructure, levels of proteins and genes involved in MPSIIIA brain pathophysiology were also investigated. ^{1}H-Magnetic Resonance Spectroscopy (MRS) indicated deficits in energetic metabolism, tissue integrity and neurotransmission at both 4 and 12 weeks in MPSIIIA mice, with partial protective effects of A5_3. *Ex-vivo* Diffusion Tensor Imaging (DTI) showed white matter microstructural damage in MPSIIIA, with noticeable protective effects of A5_3. Protein and gene expression assessments displayed both pro-inflammatory and pro-apoptotic profiles in MPSIIIA mice, with benefits of A5_3 counteracting neuroinflammation. Overall, derivative A5_3 was well tolerated and was shown to be efficient in preventing brain metabolism failure and inflammation, resulting in preserved brain microstructure in the context of MPSIIIA.

Abbreviations: MPSIIIA, mucopolysaccharidosis IIIA; HS, heparan sulfate; HPSE, heparanase; MRS, ^{1}H-Magnetic Resonance Spectroscopy; DTI, Diffusion Tensor Imaging; M_{peak}, molecular weight at peak; LMW, Low-Molecular Weight; RO heparin, periodate-oxidized, borohydride-reduced heparin; VLRO heparin, very-low-molecular weight RO heparin; PGs, proteoglycans; PAGE, polyacrylamide gel electrophoresis; GFC, gel filtration chromatography; NeuN, nuclear antigen; IL1α, interleukin −1 alpha; GFAP, glial fibrillary acidic protein; LAMP1, lysosomal associated membrane protein 1; APP, amyloid beta precursor protein; MBP, myelin basic protein; Slc1a3, excitatory amino acid transporter; NLRP3, nucleotide-binding domain and leucine-rich repeat pyrin containing protein-3; MIP1α, macrophage inflammatory protein-1 alpha; GM2a, G_{M2} activator protein; aCasp3, cleaved caspase-3; CD68, cluster of differentiation 68; Iba-1, ionized calcium binding adaptor molecule 1; cWM, medial cingulate white matter; FA, fractional anisotropy; AK, axial kurtosis; RK, radial kurtosis; Depar, diffusivity extra-axonal parallel to the fibers; Deperp, diffusivity extra-axonal perpendicular to the fibers; fin, intra-axonal volume fraction; C2, squared cosine of the angle between the fibers.

* Corresponding author at: University of Geneva, Faculty of Medicine, Department of Pediatrics, Gynecology and Obstetrics, Medical Research Foundation, 64 Avenue de la Roseraie, 1205 Geneva, Switzerland.

E-mail addresses: noemi.veraldi@unige.ch (N. Veraldi), Isabelle.DentandQuadri@unige.ch (I.D. Quadri), Yohan.VanDeLooij@unige.ch (Y. van de Looij), Corinne.Sinquin@ifremer.fr (C. Sinquin), agata.zykwinska@ifremer.fr (A. Zykwinska), Benjamin.Tournier@unige.ch (B.B. Tournier), fabien.dalonneau@ibs.fr (F. Dalonneau), honglian.li@imbim.uu.se (H. Li), Jin-ping.Li@imbim.uu.se (J.-P. Li), Philippe.Millet@unige.ch (P. Millet), romain.vives@ibs.fr (R. Vives), Sylvia.Colliec.Jouault@ifremer.fr (S. Colliec-Jouault), Ariane.Deagostini@unige.ch (A. de Agostini), Eduardo.FariasSanches@unige.ch (E.F. Sanches), Stephane.Sizonenko@unige.ch (S.V. Sizonenko).

https://doi.org/10.1016/j.carbpol.2023.121214
Received 26 April 2023; Received in revised form 13 July 2023; Accepted 17 July 2023
Available online 20 July 2023

1. Introduction

Degradation of heparan sulfate (HS) in lysosomes includes a first cut by the only known human endoglycosidase, *i.e.* heparanase (HPSE), and subsequent processing from the non-reducing end of the 5–10 kDa HS fragments by resident exoglycosidases until complete degradation of chains. Deficiency in one of the four aforementioned exoglycosidases results in mucopolysaccharidosis type III (MPSIII or Sanfilippo syndrome) that are associated with accumulation of partially digested HS oligosaccharides but also of glycosphingolipids and other macromolecules due to the impairment of the autophagosome-lysosome axis and interference in mitochondrial energy metabolism, ion homeostasis and intermediary metabolic pathways (Bruyere et al., 2015; Trudel et al., 2015). Depending on the mutated enzyme, (sulfamidase, *N*-acetylglucosaminidase, acetyl-CoA:α-glucosaminide *N*-acetyltransferase and glucosamine-6-sulfatase, respectively), MPSIII are classified in subtypes A, B, C and D (Hopwood, 1989). In general, any impairment of the autophagosome-lysosome axis is likely to cause neurodegeneration, however, MPSIII are characterized by severe and progressive neurological disorders likely to arise from the important role of HS-proteoglycans in both intracellular and extracellular processes in the central nervous system (Alexopoulou, Multhaupt, & Couchman, 2007; Zak, Crawford, & Esko, 2002; Zhang, Zhang, Wang, & Li, 2014). There is currently no cure for the neuropathology observed in MPSIII patients, and the only available treatments are symptom management and palliative support, which is debilitating and challenging for patients, parents and caregivers. Enzyme replacement therapy, gene therapy, substrate reduction therapy, hematopoietic stem cells transplantation and pharmacological chaperone therapy are active areas of research; however, at the present there is no eligible treatment for MPSIII (Pearse & Iacovino, 2020).

As an innovative approach for treating MPSIII, we hypothesize that HPSE inhibition could modify the catabolic fate of HS by preventing the lysosomal break-down of HPSE-cleaved fragments in a context of defective degradation and should be applicable to all forms of MPSIII. It is well known that glycol-split heparins are efficient inhibitors of heparanase and that inhibition of HPSE results in anti-metastatic effects (Gitay-Goren, Soker, Vlodavsky, & Neufeld, 1992; Vlodavsky et al., 1992). Glycol-split of heparin and low molecular weight (LMW) heparin dramatically decrease their anticoagulant activity while maintaining non-antithrombin-mediated biological activities (Conrad & Guo, 1992). Exopolysaccharides (EPS) excreted by deep-sea hydrothermal vent bacteria constitute another interesting class of compounds. Native EPS and, to a large extent, also their LMW highly-sulfated derivatives, have been shown to exhibit properties similar to glycosaminoglycans (Colliec Jouault et al., 2001; Zykwinska et al., 2019). They share some biological activities with heparin and on the contrary, they present a weak anticoagulant effect and carry a reduced risk of contamination by non-conventional transmissible agents owing to the substantial "species-barrier". Particularly, the EPS named diabolican (HE800 EPS), produced by the deep-sea hydrothermal vent bacterium *Vibrio diabolicus*, presents structural homology with hyaluronic acid (Rougeaux, Kervarec, Pichon, & Guezennec, 1999) and showed potent effects promoting both fibroblast proliferation and extracellular matrix production in skin substitute or dermal equivalent in an *in vitro* model (Senni et al., 2013). Its LMW highly sulfated derivative was very efficient inhibiting both proliferation and viability of various cancer cell lines (Senni et al., 2013). Another LMW highly sulfated derivative prepared from infernan (GY785 EPS), a branched slightly sulfated heteropolysaccharide synthesized by *Alteromonas infernus*, was shown to have 10 times lower anticoagulant activity than heparin and anti-metastatic properties (Colliec Jouault et al., 2001; Heymann et al., 2016). However, despite these beneficial effects, these marine compounds have not been tested in preclinical models of neurological diseases. In this study, we explored the potential use of these two marine polysaccharides together with RO heparin and a LMW analogue on the $Sgsh^{D31N}$ MPSIIIA cell line (Veraldi, Dentand Quadri, & de Agostini, 2021). Next, the diabolican derivative was selected for the treatment of the B6.Cg-$Sgsh^{(mps3a/PstJ)}$ MPSIIIA mice, in which <5 % of the wild-type level of sulfamidase is present, resulting in hepatosplenomegaly, distended bladder, brain neurodegeneration and behavioral abnormalities, similarly to humans (Bhaumik et al., 1999; Crawley et al., 2006). Using Magnetic Resonance Spectroscopy (MRS), we evaluated early brain metabolism in order to longitudinally observe the evolution of the disease. Following an eight-week treatment, we assessed the effects of A5_3 on brain metabolic alterations as well as behavioral outcomes and extent of neuroinflammation, thereby providing evidence of the potential of these polysaccharides in the context of MPSIIIA.

2. Materials and methods

2.1. Reagents and antibodies

RIPA lysis buffer, Chondroitinase ABC and DNase I, PBS 10× and Casein were purchased from Sigma Aldrich (USA). DEAE-sephacel and Sepharose-CL6B resins were from GE Healthcare. Primary antibodies used: rat LAMP1, eBio1D4B, Invitrogen; mouse NeuN, MAB377, Millipore; rabbit GFAP,Z0334, Dako; rabbit HPSE, ab288438, abcam; rabbit Iba-1, ab178846, abcam; rat CD68, 137,001, biolegend; mouse MBP, AMAB91064, Sigma; rabbit APP, ab32136, abcam. Secondary antibodies were goat anti-rabbit (Invitrogen, SA535571), donkey anti-rat (abcam, ab150149) and goat anti-mouse (abcam, ab175775) conjugated with AlexaFluor®-488, AlexaFluor®-647 and AlexaFluor®-555.

2.2. Cell culture

Primary fibroblasts from $Sgsh^{D31N}$ mice were from the Childhood Dementia Research Group (Associate Professor Kim M. Hemsley) and were cultured as reported in (Veraldi et al., 2021). Cells displayed viability higher than 96 % in all experiments, measured using the trypan blue dye exclusion method (Phillips, 1973).

2.3. Preparation of polysaccharides

RO heparin and VLRO heparin were prepared by the Ronzoni Institute (Milan, Italy) and characterized by NMR and TDA (Triple Detector Array) for the determination of the molecular weight (M) (Alekseeva et al., 2014; Bertini, Bisio, Torri, Bensi, & Terbojevich, 2005), as reported in Supplementary Figs. S1 to S4. LMW highly sulfated EPS derivatives were obtained by a free-radical depolymerization of the native diabolican produced by *V. diabolicus* (A5_3) and infernan synthesized by *A. infernus* (A5_4) followed by a sulfation reaction, as previously published (Colliec-Jouault et al., 2023; Esposito et al., 2022). Briefly, depolymerized LMW diabolican and infernan derivatives (50 mg) were dissolved in pure water and passed through a Dowex 50 WX8 column (H^+ form). After elution with pure water, the fraction was neutralized with pyridine added dropwise. After freeze-drying, LMW derivatives in their pyridinium salt forms were solubilized in dry DMF at 45 °C for 2 h under continuous stirring and then sulfated for the next 2 h at 45 °C in the presence of SO_3.py (250 mg). The final aqueous solutions (pH 7) were dialyzed against water for three days prior to be freeze-dried. Monosaccharide composition of both native EPS and their corresponding depolymerized LMW derivatives was determined together with protein impurity (Supplementary Table 1). LMW sulfated derivatives, A5_3 and A5_4, were not analyzed in term of their monosaccharide composition since sulfate groups prevent the correct derivatization and formation of the per-*O*-trimethylsilyl methyl glycosides. Weight-average molecular weight (Mw) of native EPS and their LMW derivatives was determined by High-Performance Size-Exclusion Chromatography (HPSEC, Prominence Shimadzu) coupled with a multiangle light scattering (MALS, Dawn Heleos-II, Wyatt Technology) and a differential refractive index (RI) (Optilab Wyatt technology) detectors. Samples

were eluted at 1 ml/min with 100 mM ammonium acetate. The molecular weight was calculated using a refractive index increment dn/dc of 0.145 used for polysaccharides. The linked ester sulfate group content of the native EPS and their derivatives was determined using High-Performance Anion-Exchange Chromatography (HPAEC) (Dionex DX-500) by considering the difference between the total sulfur content in the hydrolyzed sample and the initial sample (free sulfur), as previously described by (Chopin et al., 2015).

The heparanase inhibitory activity of these compounds was measured using a homogeneous time-resolved fluorescence (HTRF) assay. Heparanase was purified from the liver of transgenic mice over-expressing human heparanase (Zcharia et al., 2004). The compounds were dissolved in buffer (50 mM Tris−HCl pH 7.4, 0.15 M NaCl, 0.1 % protease free BSA, 0.1 % CHAPS) and mixed with heparanase in 384-well low-volume microplates. The assay was carried out following the instruction of the manufacturer (Cisbio Bioassays S.A.S., Codolet, France) after optimization.

2.4. Cell treatment with polysaccharides and ^{35}S-labeling

Cells were treated with 0–100 μg/ml polysaccharides in phosphate-buffered saline (PBS), pH 7.4 added twice every 48 h, for 4 days of total treatment. Cells were then rinsed with PBS and a special medium (F12 without SO_4, 10 % FBS, vitamins, inactivated BSA 0.1 mg/ml, L-glutamine, AA) was added together with the polysaccharides. 100 μCi/ml $Na_2[^{35}S]O_4$ (Hartmann Analytic, Germany) was added to favor the incorporation of radioactivity into glycosaminoglycan biosynthesis. After 24 h, culture medium was collected, cells were treated with 0.125 % trypsin/EDTA (Invitrogen) and centrifuged. Pellets were recovered and subjected to lysis with a special buffer (50 mM Tris-HCl, pH 7.2; 8 M urea; 10 mM EDTA, 1 mM PMSF, 1 mM DTT). All fractions were filtered through a 0.22 μm filter.

2.5. Isolation of heparan sulfate and analysis of the molecular weight

The detailed procedure for HS isolation is described in (Veraldi et al., 2021). Briefly, after elimination of free $Na_2[^{35}S]O_4$, final extracellular and intracellular fractions were concentrated then subjected to digestion with chondroitinase ABC and DNase I followed by β-elimination. HS was isolated by DEAE-sephacel and desalted fractions were analyzed by polyacrylamide gel electrophoresis (PAGE) and gel filtration chromatography (GFC) for the determination of the relative molecular weight (M). Polysaccharide standards with different molecular weights were used to calibrate the column (Mulloy et al., 1997).

2.6. Mouse model

Animals were bred, housed and maintained in the animal facility of the University of Lausanne (EPFL) and kept on a 12/12-h light/dark cycle with food and water *ad libitum*. All animal protocols were approved by the Swiss Federal Veterinary Service (license number VD3610) and followed the ARRIVE guidelines for animal experimentation. A colony of MPSIIIA mice (B6.Cg-Sgsh$^{(mps3a/PstJ)}$) carrying a homozygous missense mutation in the *Sgsh* gene exhibiting <5 % residual activity of sulfamidase was established. Experimentation animals were generated by heterozygote breeding and male MPSIIIA/heterozygote female crossing and were genotyped by TransnetYX using real-time PCR. Control C57BL/6 J mice were ordered from Charles River at 21 days (Saint Germain Nuelles, France). Euthanasia was performed using carbon dioxide inhalation. For DTI, histology and autoradiography techniques, mice were deeply anesthetized and transcardially perfused with PBS. Brains were removed and the right hemisphere was immersed in a 4 % paraformaldehyde PBS solution for 6 weeks (for DTI), then cryopreserved in 30 % sucrose/PBS for 48 h at 4 °C before storing at −80 °C for histological analysis; the left hemisphere was snap frozen (for autoradiography). For WB and RT-qPCR analyses, mice were deeply anesthetized, brains were removed, hemispheres split and structures (cortex and hippocampus) snap frozen and kept at −80 °C. Organs including liver, spleen, and kidney were removed, snap frozen and kept at −80 °C. Behavioral assessments were carried out on half the controls and all the MPS mice (n = 7–12 mice per group). Histology and biochemistry were carried out on n = 5–7. Animals and samples were assigned identification numbers to minimize subjective bias.

2.7. Animal treatment

The administration route for compounds was intraperitoneal injection. Male and female mice in an expected ratio 1:1 (observed 64%F, 36%M) were divided in four groups (Control, MPSIIIA, MPSIIIA$_{A5_3}$ and MPSIIIA$_{placebo}$) and MPSIIIA$_{A5_3}$ group was treated with A5_3 at 20 mg/kg, 3 times per week and during 8 weeks. Since A5_3 treatment of Sgsh$^{+/+}$ cells did not impact HS turnover, control mice treated with A5_3 were not included in this set of experiments. No effect of sex was observed in this set of experiments. For statistical analysis, results from the groups MPSIIIA and MPSIIIA$_{placebo}$ were merged due to lack of a significant difference between them.

2.8. Magnetic resonance spectroscopy

Mice were continuously anesthetized under 1.5–2 % isoflurane flow for the duration of the experiments. Body temperature was maintained at 37 °C using a thermoregulated water circulation system placed on the back of the mouse. Respiration and heart rate were also monitored during the acquisition. MRS experiments were performed on a 9.4-T/31-cm magnet (Magnex Scientific, Abington, UK) connected to Direct Drive console (Varian, Palo Alto, CA) equipped with 12-cm gradient coils (400 mT/m, 120 msec). A homebuilt 17-mm-diameter ^1H quadrature surface coil was used for radiofrequency transmission and signal reception. Measurements were performed on 4 and 12-week-old mice according to (van de Looij, Chatagner, Huppi, Gruetter, & Sizonenko, 2011). A Fast Spin Echo T2W image was performed to position ^1H-MRS voxels of interest. ^1H-MRS spectra acquisition were performed on the cortex (voxel of interest of 1.5 × 1.5 × 2.5 mm^3) and hippocampus (voxel of interest of 1.5 × 2.5 × 2.5 mm^3) using an ultrashort echo time (TE/TR = 2.7/4000 ms) SPECIAL spectroscopy method (Mlynarik, Gambarota, Frenkel, & Gruetter, 2006). After automatic FASTMAP shimming (Gruetter & Tkac, 2000), spectra were acquired in 24 blocks and 20 blocks of 16 averages for cortex and hippocampus, respectively. LC-Model (Provencher, 1993) was used to analyze the acquired spectra and quantify cerebral metabolites described in Results.

2.9. Diffusion Tensor Imaging (DTI)

Ex vivo MRI experiments were performed on a 14.1 T magnet (Bruker) with a homemade saddle coil of 2 cm diameter. A multi-b-value shell protocol was acquired using a spin-echo sequence (FOV = 21 × 16 mm2, matrix size = 128 × 92, 12 slices of 0.6 mm, 3 averages with TE/TR = 45/2000 ms). 89 DWI were acquired, 5 b0 images and 84 separated in 3 shells (noncollinear and uniformly distributed in each shell) with number of directions/b-value in s/mm^2: 28/2000, 28/4000 and 28/5000. Acquired data were fitted using the white matter tract integrity model based on diffusion kurtosis imaging (DKI) (Jespersen, Olesen, Hansen, & Shemesh, 2018). Cortex (CX), external capsule (EC), and medial cingulate white matter (cWM) were assessed. DTI derived parameters (Axial diffusivity (AD), Radial diffusivity (RD), Mean diffusivity (AD) and Fractional anisotropy (FA)), DKI derived metrics (mean (MK), axial (AK), and radial (RK) kurtosis) as well as WMTI derived metrics axial and radial diffusivity in the extra axonal space (Depar and Deperp, respectively), intraxonal diffusivity (Daxint), intra-axonal volume fraction (fin) and C2 (the square of the cosine of the angle between the fibers considered as the fanning of the fibers) were averaged in the different regions assessed for all animals.

2.10. Behavioral assessment

Open field, Y-maze, Beam Balance and Hang Wire tests were carried out in a room maintained under constant light, temperature, and humidity. Mixed female and male animals were habituated to the testing room for at least 30 min and the same investigators performed the tests during daylight hours (between 9 a.m. and 5 p.m.). Behavior was recorded and analyzed in a blinded fashion once all tests had been performed. A 30-min room adjustment period was implemented before the start of each test. All values are expressed as means ± standard error. The Open Field test (Bailey & Crawley, 2009) was used to assess anxiety behavior and is a general assessment of animal basal locomotor activity and exploration (Prut & Belzung, 2003). Animals were individually placed in the center of an arena (43 × 50 cm, white Plexiglas) divided into central and peripheral areas and left to explore freely for a total of 10 min, the first 5 min of which were used for analysis. ANY-MAZE Video Tracking System version 7.10 (Stoelting Europe) was used to assess motor activity, exploratory drive and anxiety. Parameters assessed include total time spent in the center and the periphery, and percent time moving, resting and grooming, number of rearings and crossings. The Y-maze test is used to evaluate memory and exploratory behavior of rodents (Wolf, Bauer, Abner, Ashkenazy-Frolinger, & Hartz, 2016) that typically prefer to investigate a new arm of the maze rather than returning to one that was previously visited. One of the three arms was blocked and the animal was able to explore only two arms for 5 mins, after which the block was removed, and the animal had another 5 min to explore all three arms (T2). Percentage of time spent in the novel arm was calculated. Alternations were defined as percent using the formula = [number of alternances/(total number of arm entries– 2)] x 100 (Gleitz, O'Leary, Holley, & Bigger, 2017). Beam Balance evaluates motor coordination and balance. During training, animals were encouraged to cross two wooden beams (a square-shaped and round ones), elevated 30 cm above the ground, until reaching a familiar item from their housing box on the other end of the beam. After 24 h, animals were given three trials to cross each beam and a maximum of 60 s was allowed for the crossing. Parameters analyzed included: time to cross beam in seconds for each trial, number and side of hind paws slips. The Hang Wire test was performed to assess motor strength according to previous protocol (Hasegawa et al., 2017) with a metallic wire (2 mm diameter) suspended 30 cm from the ground. The latency was recorded until the animal fell from the mesh for a maximum of 60 s. The mean time for three trials was assigned for each mouse.

2.11. Autoradiography

Brain sections (20 μm) were cut using a cryostat (Leica Biosystems, Buffalo Grove, IL) and mounted in series in Superfrost slides for SPECT analysis. Slices were first immersed in 1× PBS (30 min), then in radioactive buffer (90 min) and then rinsed twice in 4 °C Tris-$MgCl_2$ buffer (3 min) and briefly washed in cold water. CLINDE was obtained as previously described in detail (Tournier et al., 2020) Radioactive buffer: Tris-$MgCl_2$ buffer (50 mM Tris HCl, 50 mM $MgCl_2$, pH 7.4) containing [^{125}]-CLINDE (0.11 MBq/ml) alone or in presence of 10 μM of unlabeled CLINDE to determine the non-specific binding. Slides were air-dried before exposure onto gamma-sensitive phosphorimaging plates (Fuji BAS-IP MS2325) for 30 min. Brain sections were then stained with cresyl violet to delineate regions of interests (ROIs) in the cortex and anterodorsal hippocampus. Autoradiograms were analyzed using Fujifilm BAS-1800II phosphorimager using Aida Software V4.06 (Raytest Isotopenmessgerate GmbH) in presence of homemade ^{125}I calibration curves. Specific binding ratio (SBR) was calculated as follows: (Average radioactivity in ROI over 12 sections/radioactivity in ROI over 4 slices in the presence of 10 μM of unlabeled radiotracer) – 1. For each radiotracer, quantification was performed individually on the ROI.

2.12. Western Blot

Frozen tissue was homogenized on ice in RIPA lysis buffer containing protease inhibitors (Sigma-Aldrich) and total proteins were quantified using Bradford (Bio-Rad). Samples were electrophoresed through a 4–12 % acrylamide SDS-PAGE by loading equal amounts of proteins (25 μg) on a Bio-Rad Mini-PROTEAN TGX Stain-Free Gel (Bio-Rad). Proteins were transferred to nitrocellulose membranes and detected with either overnight incubation at 4 °C or 1 h at room temperature of primary antibodies (1:1000 in blocking buffer containing 0.1 % casein) followed by 2 h incubation at room temperature with a fluorescent secondary antibody (1:10,000), conjugated with either DyeLight™-800 or AlexaFluor®-680. Detection was achieved using iBright reader (Thermo Fisher) and densitometric protein band quantification was performed with Image Studio™ Lite software (LI-COR Biosciences). The optical density of each sample was first estimated based on the optical density of a loading control (Actin) and then expressed as a percentage of the control group (100 %).

2.13. RT-qPCR

Total RNA was extracted using Quiagen Mini RNA kit from 30 mg of tissue. 3 μg RNA were retrotranscribed into cDNA with random hexamers (Promega), dNTP (Promega), RNAsin, DTT and M-MLV reverse transcriptase (Invitrogen). Quantitative PCR was performed using 15 ng of cDNA, 2× SYBR-Green Master Mix (PowerUp®, Invitrogen) on the QuantStudio™ 5 System and elaborated with the Design&Analysis Software 2.5.1 (Thermo Fisher). Amplification parameters: 95 °C for 2 min, (95 °C for 15 s, 58 °C for 1 min) X 40 cycles, 58 °C for 5 s, 65 °C for 10 s, 95 °C for 30 s. Negative controls included omission of reverse transcriptase at the cDNA synthesis step and omission of the template at the PCR step. Additional controls performed for each cDNA amplification included assessment of amplification efficiency and detection of possible primer dimerization through analysis of dissociation curves. Ct (Cycle threshold) values were determined as the numbers of PCR cycles at which specific amplification of the target sequence occurred. Ct superior to 35 were considered as background signal. Fold changes in gene expression were calculated as the ratio of molecules of the target gene against the housekeeping gene (rps18), *via* $\Delta\Delta C_T$ analysis. Each sample was analyzed in duplicate. Primers: rps18, forward: 5′- CCGCCATGTC TCTAGTGATCC-3′, reverse: 5′- GCCCATCGATGTTGGTGTTG-3′; Slc1a3, forward: 5′- CAGTCTCGTCACAGGAATGGC-3′, reverse: 5′- ATAGACTA-CAGCGCGCATCC-3′; Slc2a1, forward: 5′- GGATCCCAGCAGCAAGAA GG-3′, reverse: 5′- AGCCGAACTGCAGTGATCC-3′; IL1α, forward: 5′-CGTGTTGCTGAAGGAGTTGC-3′, reverse: 5′- TCCAGAAGAAAATGAGG TCGGT-3′; GM2a, forward:5′- ATCGCCATGCACCGTCTAC-3′, reverse: 5′-AGTTGGGAAAGGCGCTTCG-3′; LAMP1, forward: 5'-CGTGAGCTGC-CACTTTCCTA-3′, reverse: 5′- AACGCCAACACAAGACTGGA-3′; MIP1α, forward: 5'-CAGCCAGGTGTCATTTTCCTGA-3′, reverse: 5'-TCTTGGAC CCAGGTCTCTTTG-3′; TLR4, forward: 5'-AATCCCTGCATAGAGGTA GTTCC-3′, reverse: 5′- TCATCAGGGACTTTGCTGAGTT-3′; NLRP3, forward: 5'-CTTCTGCACCCGGACTGTAA-3′, reverse: 5′- CTGCAGTTGTC-TAATTCCAGCAT-3′; HPSE, forward: 5′- TTTGCAGCTGGCTTTATGTGG-3′, reverse: 5′- ACCTGCCTCATCACGACTTC-3′.

2.14. Immunohistochemistry

Brain sections (20 μm) were cut using a cryostat (Leica Biosystems, Buffalo Grove, IL) and mounted on Superfrost® slides. Immunohistochemistry was performed on sections encompassing cortex and anterodorsal hippocampus according to the Allen mouse brain atlas (Langford-Smith et al., 2011; Malinowska et al., 2010). Regions of Interest assessed were: motor cortex (M1), somatosensory cortex (S1), hippocampus (CA1) and in the medial cingulate white matter (cWM). The regions were chosen to match the same regions evaluated by *ex vivo* DTI. Images were acquired with Nikon Eclipse T2000 microscope system

coupled to a DSQ/QI2 camera (Japan) at 20 and 40× magnification, processed with NIS Elements (Nikon, Japan) and quantified with ImageJ (NIH) software as previously described (Sanches et al., 2021).

2.15. Structural characterization of heparan sulfate from the prefrontal cortex

Frozen prefrontal cortex was homogenized on ice in 400 µl PBS and total proteins were quantified using Bradford (Bio-Rad). Heparan sulfate was purified by Proteinase K (20 mg/ml, Eurobio) digestion at 55 °C followed by inactivation at 95 °C and centrifugation at 10000 rpm for 10 mins. Supernatants were loaded onto a diethylaminoethanol-sephadex column (GE Healthcare) and eluted with increasing NaCl concentrations. The 1.5 M fraction was concentrated, desalted and exhaustively depolymerized using a cocktail of heparinase I, II and III (10 mU each, 48 h at 37 °C). Disaccharides were quantified by RPIP-HPLC as reported in (Henriet et al., 2017).

2.16. Sulfatase activity assay

Recombinant HSulf-2 was expressed and purified as previously described (Seffouh et al., 2019). For functional assays, heparin (25 µg) was digested with Hsulf-2 (2 µg) for 24H at 37 °C in 50 mM Tris, 2.5 mM $MgCl_2$ pH 7.5, in the presence of increasing concentrations of A5_3 and A5_4 inhibitors (0–10 µg/ml). After heating, aliquots of heparin (450 ng) were resuspended in 100 mM sodium acetate pH 7.1, 0.5 mM calcium acetate, and exhaustively depolymerized using a cocktail of heparinase I, II and III (10 mU each, 48 h at 37 °C). Heparin content in [ΔHexA,2S-GlcNS,6S] and [ΔHexA,2S-GlcNS] disaccharides (HSulf-2 disaccharide substrate and product, respectively) were determined by RPIP-HPLC analysis (Henriet et al., 2017), using NaCl gradients calibrated with authentic standards (Iduron). Results are expressed as the [product]/[substrate] ratio.

2.17. Statistical analysis

Data are expressed as means ± standard deviation or standard error depending on the parameter, as specified. Statistical analysis was performed using GraphPad Prism 9.4.1 and IBM SPSS 22.0 for Windows. Data distribution normality was tested using the Kolmogorov-Smirnov test. Student's *t*-test or Mann-Whitney, Multiple Student's t-test with Bonferroni-Dunn *post hoc*, one-way ANOVA (with Tukey's *post hoc* for multiple comparison) or Kruskall-Wallis followed by Dunn's test were used when appropriate. $p < 0.05$ value was considered significant.

3. Results

3.1. Effects of treatment on MPSIIIA fibroblasts

3.1.1. Distribution of heparan sulfate

Heparin derivatives with reduced anticoagulant activity and marine LMW sulfated polysaccharides (Table 1) have been investigated for their possible use in Sanfilippo syndrome. LMW sulfated derivatives, A5_3 and A5_4, were prepared, respectively, from native diabolican and infernan EPS through a two-step process (Colliec-Jouault et al., 2023; Esposito et al., 2022). In agreement with our previous studies, monosaccharide composition and sulfur content of both native EPS and their corresponding LMW derivatives indicated that depolymerization reaction had no major impact on the polysaccharide structure (Table S1). Furthermore, recent NMR analyses allowed to determine that sulfation reaction led to a fully sulfated LMW diabolican derivative (Fig. 1A), while LMW sulfated infernan has more heterogenous structure with sulfate groups distributed in both backbone and side chain (Fig. 1B). To facilitate the polysaccharides to reach the brain through blood brain barrier (BBB), sulfated diabolican (A5_3) and infernan (A5_4) derivatives of low-molecular weights, respectively 5.5 kDa and 8 kDa were selected for this study. In parallel, very-low-molecular weight RO heparin (VLRO heparin, 3.3 kDa) and RO heparin (16.5 kDa) were used as references (Fig. 1C and D). The sulfate content of all four polysaccharides used was similar (Table 1).

Table 1
Main features of LMW polysaccharides: weight-average molecular weight (Mw), number-average molecular weight (Mn), polydispersity (Mw/Mn), sulfate content (% sulfate) and heparanase (HPSE) activity.

Polysaccharide	Type	Mw (kDa)	Mn (kDa)	Mw/Mn	% Sulfate	HPSE activity*
A5_3	Diabolican (HE800 EPS) derivative	5.1	3.7	1.4	40	10–50
A5_4	Infernan (GY785 EPS) derivative	8.3	6.0	1.38	36	10–50
VLRO heparin	Heparin derivative	3.3	2.8	1.19	30	nd
RO heparin	Heparin derivative	16.5	9.8	1.67	30	<0.1

* IC50 µM; nd, not determined.

To evaluate the distribution of proteoglycans (PGs) during their biosynthesis in untreated and polysaccharide-treated MPSIIIA fibroblasts, $Na_2[^{35}S]O_4$ (a radiolabeled sulfate donor) was incorporated. Cells were counted at each experiment and results were normalized to the number of cells. Correction for the $^{35}SO_4$ incorporation level (the ratio between recovered measured total radioactivity and the initial radioactivity administered to cells, ranging from 1.2 % to 5.6 % in this set of experiments) was performed. We chose to first treat cells with 100 µg/ml polysaccharides, which corresponds approximately to the IC50 value for A5_3/A5_4. Upon results, two lower concentrations were also tested (50 and 20 µg/ml). Treatment did not alter significantly the proportion of extracellular and intracellular PGs produced by cells (Fig. S5). Heparan sulfate represents a fraction of total glycosaminoglycans and the proportion of PGs bearing HS is variable. This percentage was found to span from 12 to 28 % in untreated cells, in agreement with our previous study (Veraldi et al., 2021), while it varied from 18 to 46 % in treated cells (Fig. S6). HS was isolated from both extracellular and intracellular fractions and the percentage of HS on total incorporated radioactivity (PGs) was also calculated. The increase in the extracellular fraction of HS observed upon treatment with 100 µg/ml A5_4 was not significant and cell treatment with polysaccharides did not evidently alter the total amount and distribution of proteoglycans and HS.

1.1.1. Determination of the molecular weight (M) of heparan sulfate

We next looked for possible effects of polysaccharide treatment on the length of HS chains, which would indicate an inhibition of the first step in HS degradation, *i.e.* heparanase action, resulting in HS chains with a different M_{peak} and/or distribution. For this, cells were treated for four days before adding the radioactive sulfate donor and fractions were collected after 24 h. The estimation of the size of HS in untreated cells and upon treatment with 20 µg/ml of the four polysaccharides was performed by both PAGE and gel filtration chromatography (GFC) and is summarized in Table 2. As previously reported (Veraldi et al., 2021), extracellular HS was concentrated in the high-molecular weight region, with an average M_{peak} of 37.1 ± 2.3 kDa by PAGE ($n = 8$) and 43 ± 8.6 kDa by GFC ($n = 3$). In contrast, intracellular HS exhibited a broad distribution of partially degraded HS fragments of 7.9 ± 2.3 kDa M_{peak} -resolved only by GFC. Upon treatment with the four polysaccharides, the M of extracellular HS was not altered, while a well resolved peak of intracellular HS appeared, corresponding to more homogeneous species. Specifically, a shift towards higher molecular weight (> 20 kDa) was clearly observed with reduced presence of LMW fragments, suggesting decreased degradation of HS in accordance with HPSE inhibition. Similar results were obtained between the three concentrations of

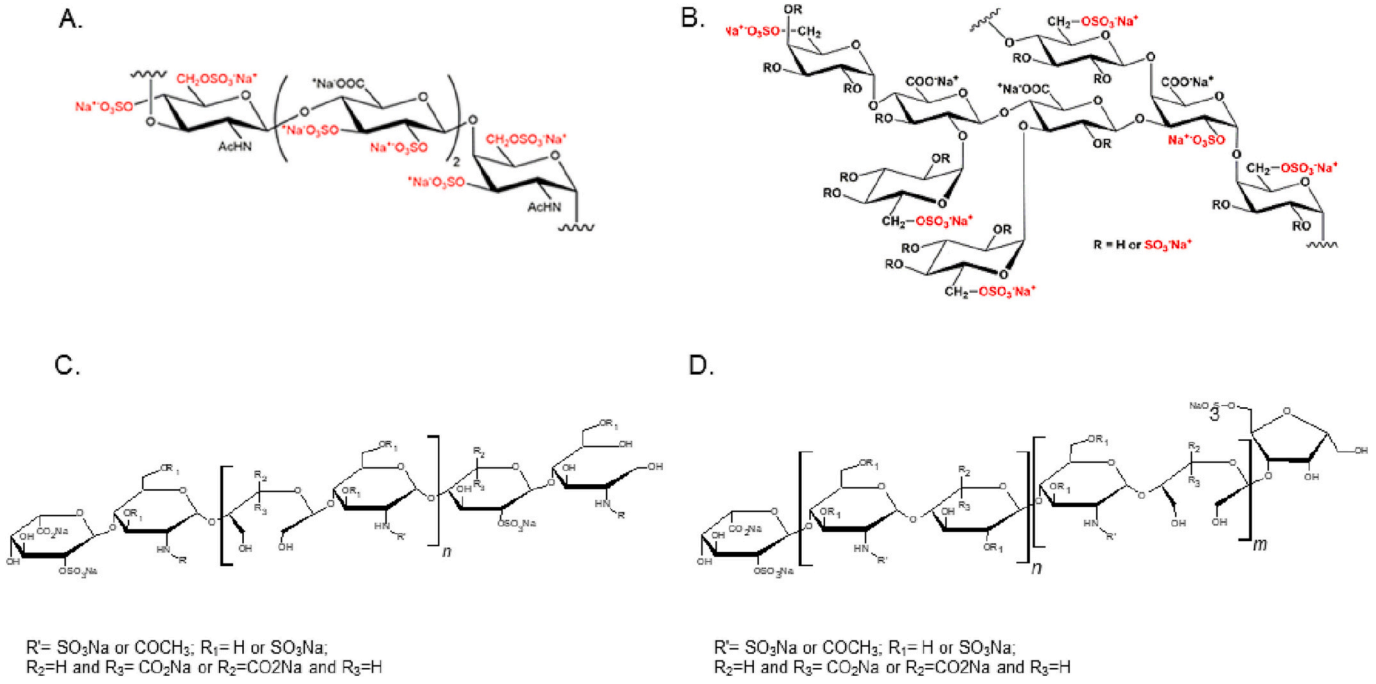

Fig. 1. Structure of polysaccharides. (A) Tetrasaccharide repeating unit of diabolican EPS (Esposito et al., 2022; Rougeaux et al., 1999). (B) Octasaccharide repeating unit of infernan EPS (Roger et al., 2004; Colliec-Jouault et al., 2023). Sulfated positions in LMW sulfated derivatives are indicated in red. C) Repeating units of RO heparin and (D) very low RO heparin (VLRO heparin).

Table 2
Size distribution of HS in MPSIIIA cells treated with 20 μg/ml HPSE inhibitors. HS was isolated from control and treated cells and analyzed by PAGE and GFC. The molecular weight (M) is expressed in kDa. When possible, the average of two independent analyses ± SD is reported. The range is calculated at half peak height.

	PAGE				GFC			
Sample	Intracell		Extracell		Intracell		Extracell	
	M_{peak}	M_{range}	M_{peak}	M_{range}	M_{peak}	M_{range}	M_{peak}	M_{range}
Untreated*	Smear	Smear	37.1 ± 2.3	24–50.7	7.9 ± 2.3	3.5–28	43 ± 8.6	17.7–116.7
A5_3	33.5 ± 1.1	18.8–51.1	42.2	24.2–60.3	36.5 ± 2.7	12.8–91.8	49.6	20.2–141.5
A5_4	34.9 ± 5	23.4–50.8	35.5 ± 0.7	24.9–49.2	40.6 ± 0.1	16.2–113	41.2	16.2–116.2
VLRO	32.1 ± 1	11.8–50.4	37.2 ± 5.6	27.3–50.3	15.6	4.3–113	49.9	17.1–128.8
RO	28.5 ± 3.4	17.5–37.9	34.5	24.7–41.7	18.5	4.8–78.6	46.2	16.7–157.7

* Previously published in (Veraldi et al., 2021).

polysaccharides tested (Table S2 and Fig. S7) and as shown in Fig. 2 for A5_3. A lower concentration of A5_3 (10 μg/ml) was also tested (Fig. S8 and Table S3); however, as expected, the effect was more pronounced with higher doses. Based on the data obtained from cell culture experiments, we chose to explore the effects of repeated administration of A5_3 derivative from *V. diabolicus* on the MPSIIIA mouse model due to its lower molecular weight and higher sulfate content in comparison to A5_4. About the dosage, due to the scarcity of data regarding animal treatment protocols with EPS derivatives we looked for data on the use of LMW heparins in neurodegenerative diseases. A paper by Bergamaschini et al. reports that IP administration of 60 μg/mouse enoxaparin three times a week for 6 months was well tolerated and prevented the deposition of b-amyloid in transgenic mice overexpressing APP23 (Bergamaschini et al., 2004). In addition, clinical trials reported the safety of *N*-acetylated RO heparin (Roneparstat) up to 400 mg/day in humans (Galli et al., 2018). A toxicology study commissioned by the group of Dr. Colliec-Jouault showed that 2-week IV treatment with 10 and 30 mg/kg EPS derivatives was safe (confidential data). We therefore decided to treat MPSIIIA mice by IP injections three times a week with the lowest effective dosage observed in cells (20 mg/kg).

3.2. *In vivo brain metabolism assessment by MRS*

Quantification of metabolites in both cortex and hippocampus was performed for controls, MPSIIIA treated and MPSIIIA non-treated animals to obtain the brain neurochemical profile of mice. ^{1}H-MRS revealed noticeable metabolic changes in the cortex of 4-week-old MPSIIIA mice compared to control animals (Fig. 3, panels in A): decreased concentration of glutamate (ctrl *vs* MPSIIIA, Glu, $p = 0.009$), glycine (Gly, $p = 0.02$), glucose (Glc, $p < 0.001$), creatine+phosphocreatine (Cr + PCr, $p < 0.001$) myoinositol (Ins, $p = 0.03$), taurine (Tau, $p = 0.01$), macromolecules (Mac, $p < 0.001$), *N*-acetyl aspartate (NAA, $p < 0.001$), and *N*-acetyl aspartate+*N*-acetylaspartyl glutamate (NAA + NAAG, $p < 0.001$). At 12 weeks, less alterations were observed comparing control with untreated and treated MPSIIIA animals (Fig. 3, panels in B): decreased lactate ($p = 0.006$), Glu/Gln ($p = 0.0067$), PE ($p = 0.0098$), Lac/(NAA + NAAG) ($p = 0.004$), PCr/Cr ($p = 0.0496$), some partially reversed upon treatment with A5_3. The hippocampus was less sensible to metabolic alterations at 4 weeks (Fig. 3, panels in C), however Lac (ctrl *vs* MPSIIIA, $p = 0.02$), Glc ($p = 0.001$), Cr + PCr ($p = 0.01$), Tau ($p = 0.03$) and Mac ($p = 0.02$) were all decreased in MPSIIIA mice. At 12 weeks, (Fig. 3, panels in D) a significant decrease in the levels of Glu/Gln ($p = 0.0009$), Tau ($p = 0.0008$) (reversed by A5_3), PE ($p = 0.0012$) was observed

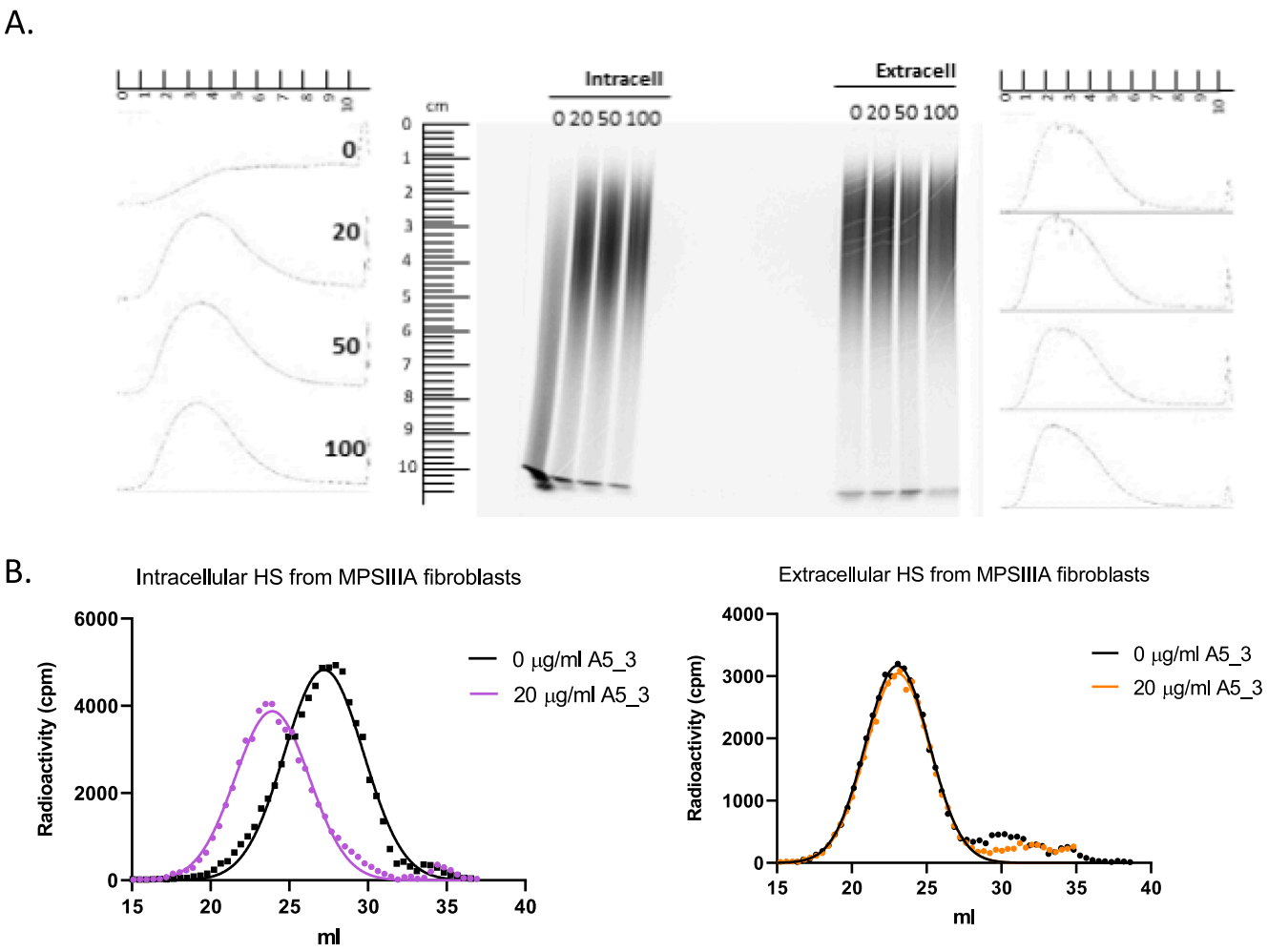

Fig. 2. The molecular weight (M) of intracellular HS is altered in MPSIIIA fibroblasts upon treatment with A5_3. Panel A: HS was isolated from control (0 µg/ml A5_3) and cells treated with 20–50-100 µg/ml A5_3, analyzed by PAGE and detected by autoradiography 300,000 cpm of HS were loaded on the gel. The relative molecular weight (M) is calculated by comparison with a standard curve. Profiles were obtained with the software ImageJ. Panel B: on the left, superimposition of the GFC profiles of intracellular HS from control (0 µg/ml A5_3) and cells treated with 20 µg/ml A5_3. Treatment causes a shift towards higher M. On the right, superimposition of the GFC profiles of extracellular HS from control and treated cells. The relative M reported in the main text was calculated by comparison with a standard curve. 75,000 cpm of HS were applied to the column.

together with increased NAAG ($p = 0.007$). Taken together, MRS data evidenced an early disruption of brain metabolism (as early as 4 weeks of age) in MPSIIIA mice, which may represent a starting point for the neurodegeneration observed at a later timepoint.

3.3. Behavioral tests

For characterizing the phenotype of MPSIIIA mice, functional tests were performed at 11 weeks of age. Differences were observed between control and MPSIIIA mice in the Open Field and in the Beam Balance tests. In the Open Field test (Fig. 4, panels in A), MPSIIIA mice showed reduced distance covered ($p < 0.0001$), reduced number of crossings ($p = 0.0035$) and average speed ($p < 0.0001$) compared to controls. Specifically, mice tended to move less, both in the center (reduced distance, $p = 0.0005$; reduced speed, $p < 0.0001$) and in the periphery (reduced speed, $p < 0.0001$). Upon treatment, no significant changes were observed. In the Beam Balance test (Fig. 4, panels in B), MPSIIIA mice were shown to be faster than controls in crossing the bar ($p = 0.005$) and no difference in the hindlimb errors while crossing the beam was observed. Interestingly, A5_3 treatment partially improved the performance of the animals in this task, as shown by the reduced errors/time ratio where MPSIIIA failed more than controls ($p = 0.0289$).

3.4. Neuropathology markers

The expression of proteins involved in neuroinflammation was quantified by Western Blot (Fig. 5, panels A and B). Increased GFAP was observed in the cortex of MPSIIIA ($p = 0.009$) with no effects of A5_3 treatment on astrogliosis. The expression of cleaved caspase-3 (aCasp3) was not altered, however, increased total caspase3 (Casp3) was detected ($p = 0.0008$), suggesting a pro-apoptotic profile in MPSIIIA mice. Increased expression of the lysosomal marker LAMP1, associated with lysosomal expansion, was observed both in the cortex ($p = 0.0041$) and the hippocampus ($p = 0.002$) of MPSIIIA mice with a slight effect of treatment.

The transcription level of genes potentially involved in MPSIIIA neuropathology was measured by RT-qPCR (Fig. 5, panels C—F). Increased mRNA expression of HPSE was detected in both cortex and hippocampus ($p = 0.0067$ and $p < 0.0001$, respectively). Upon MRS results, we also looked at the excitatory amino acid transporters Slc1a3 and Slc2a1 and observed decreased Slc1a3 mRNA level in the cortex ($p = 0.011$) but not in the hippocampus. Secondary accumulation of GM2 and GM3 gangliosides, which are postulated to alter axon morphology and synaptic transmission (Clarke, 2008), was shown in MPSIIIA animal models (Crawley et al., 2006; Martins et al., 2015; Wilkinson et al., 2012). We did not directly measure GM2 levels, rather we analyzed the

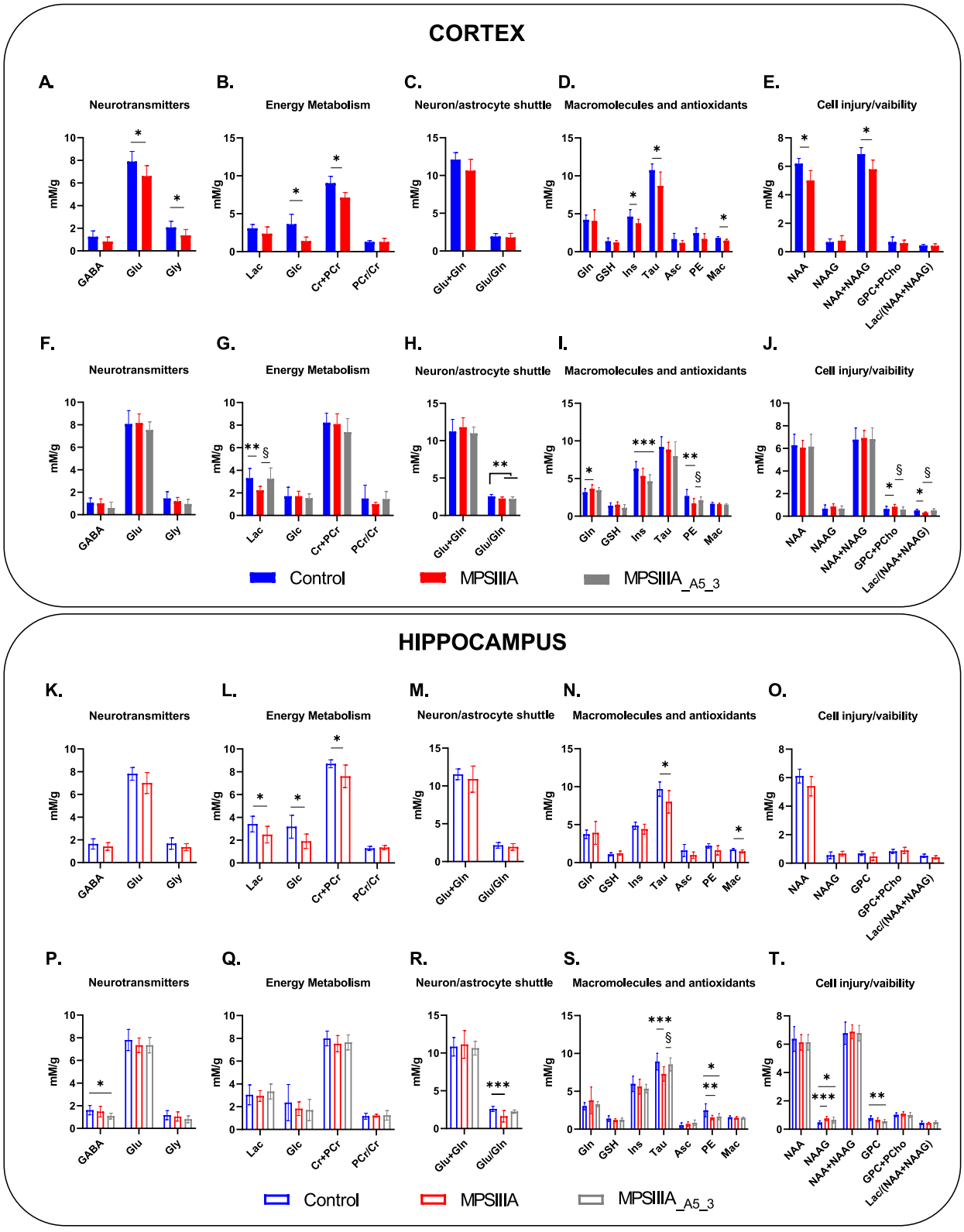

Fig. 3. Brain metabolism assessed by ^{1}H-MRS in the cortex and hippocampus of control and MPSIIIA mice. Quantification of metabolites in the cortex of 4-week-old mice (panels A-E: control, $n = 12$ *vs* MPSIIIA, $n = 20$) and of 12-week-old mice (panels F-J: control, n = 12 *vs* MPSIIIA, $n = 11$, treated MPSIIIA, $n = 10$). Quantification in the hippocampus of 4-week-old mice (panels K—O, control, n = 12 *vs* MPSIIIA, $n = 22$) and of 12-week-old mice (panels P-T, control, $n = 13$ *vs* MPSIIIA, n = 12, treated MPSIIIA, n = 10). Creatine (Cr), phosphocreatine (PCr), γ-aminobutyric acid (GABA), glutamine (Gln), glutamate (Glu), Glutathione (GSH), glycine (Gly), myo-inositol (Ins), lactate (Lac), *N*-acetylaspartate (NAA), taurine (Tau), ascorbate (Asc), glucose (Glc), *N*-acetylaspartylglutamate (NAAG), macromolecules (Mac), phosphatidylethanolamine (PE), glycerophosphocholine (GPC), phosphocholine (PCho). Significance testing was determined using multiple student's *t*-test or one-way ANOVA. * Control *vs* MPSIIIA; §MPSIIIA *vs* MPSIIIA treated with A5_3.

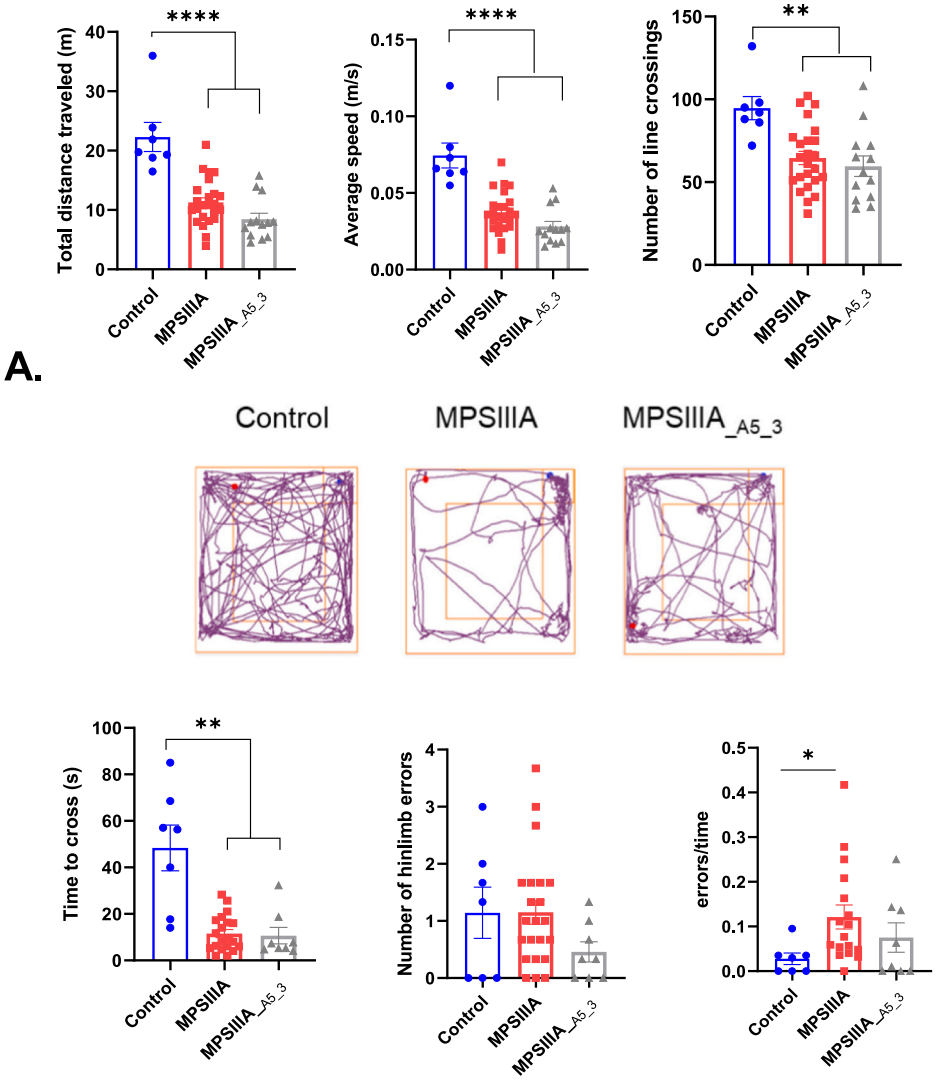

Fig. 4. Behavioral alterations in MPSIIIA mice. Both male and female mice were subjected to different behavioral tests at 11 weeks of age. A) Significant decrease in total distance traveled, average speed and number of line crossings in the Open Field test by MPSIIIA mice compared to controls. Representative images of the locomotor activity are reported below the graphs. B) Significant decrease in the time to cross the beam and increased errors/time by MPSIIIA mice compared to controls in the Beam Balance test. Significance testing was determined using one-way ANOVA. Data are expressed as mean ± SEM. *$p < 0.05$, ** $p < 0.01$, ****$p < 0.0001$.

level of transcription of GM2 activator protein (GM2a), which is an essential cofactor for the degradation of GM2 gangliosides. Indeed, increased levels of GM2a align with increased lysosomal biogenesis. mRNA levels of the lysosomal proteins LAMP1 and GM2a were significantly altered in the hippocampus ($p = 0.005$ and $p = 0.0155$, respectively), but not in the cortex of our model. Increased IL-1α and MIP-1α have been observed in MPSIII mouse brains (Guo, DeAngelis, Zhu, Schuchman, & Simonaro, 2019; Holley et al., 2018; Wilkinson et al., 2012), correlating to microglial cell priming involving TLR4 and MyD88 in 3-month-old MPSIIB (Fu et al., 2017). Accordingly, we detected increased macrophage inflammatory protein MIP1α in both cortex and hippocampus ($p = 0.0001$) together with interleukin-1α (IL-1α, $p < 0.0001$, with an effect of treatment), along with no difference in the inflammasome component NLRP3. Treatment differently altered the transcription of TLR4 in cortex and hippocampus ($p = 0.0038$ and $p = 0.018$, respectively).

Protein expression was also studied by immunostaining in the cortex (M1 and S1 regions) and hippocampus (CA1) but no significant difference in optical density (ODI) could be observed for LAMP1, HPSE and NeuN (Fig. S9), GFAP (Fig. S10) and the microglia marker Iba-1 (Fig. S11). Treatment impacted the expression of the monocyte marker CD68 (Cluster of Differentiation 68) in the CA1 region ($p = 0.029$) (Fig. S11, panel d). Interestingly, a significant increase in amyloid beta precursor protein (APP) in the CA1 region ($p = 0.0352$) and decreased expression of myelin basic protein (MBP) in the cortical S1 region ($p = 0.009$) of MPSIIIA mice were detected, both reversed by A5_3 treatment (Fig. 6, panels C and F). Overall MPSIIIA mice at 12 weeks presented with altered levels of some inflammatory markers with indication of axonal injury in specific areas of the brain (Beard et al., 2017), reversed upon treatment.

3.5. Brain microstructure assessment by Advanced Diffusion Imaging

Diffusion tensor imaging (DTI), diffusion kurtosis imaging (DKI) and white matter tract integrity (WMTI) models were used in this study in order to evaluate the integrity of brain microstructure (Fig. 7). In MPSIIIA mice, fractional anisotropy (FA) was decreased in the external capsule ($p = 0.04$) and medial cingulate white matter (cWM, $p = 0.03$) compared to controls, as well as axial kurtosis (AK) in both the motor cortex ($p = 0.02$) and cWM ($p = 0.04$). These effects were reversed by A5_3 treatment in the cWM. Radial kurtosis (RK) was decreased in MPSIIIA brains in the motor cortex ($p = 0.002$), external capsule ($p = 0.007$) and cWM ($p = 0.0008$). A5_3 reversed tissue damage only in the cWM. MPSIIIA mice presented with decreased extra-axonal diffusivity perpendicular to the fibers (Deperp) in the somatosensory cortex ($p = 0.005$) and increased extra-axonal diffusivity parallel to the fibers

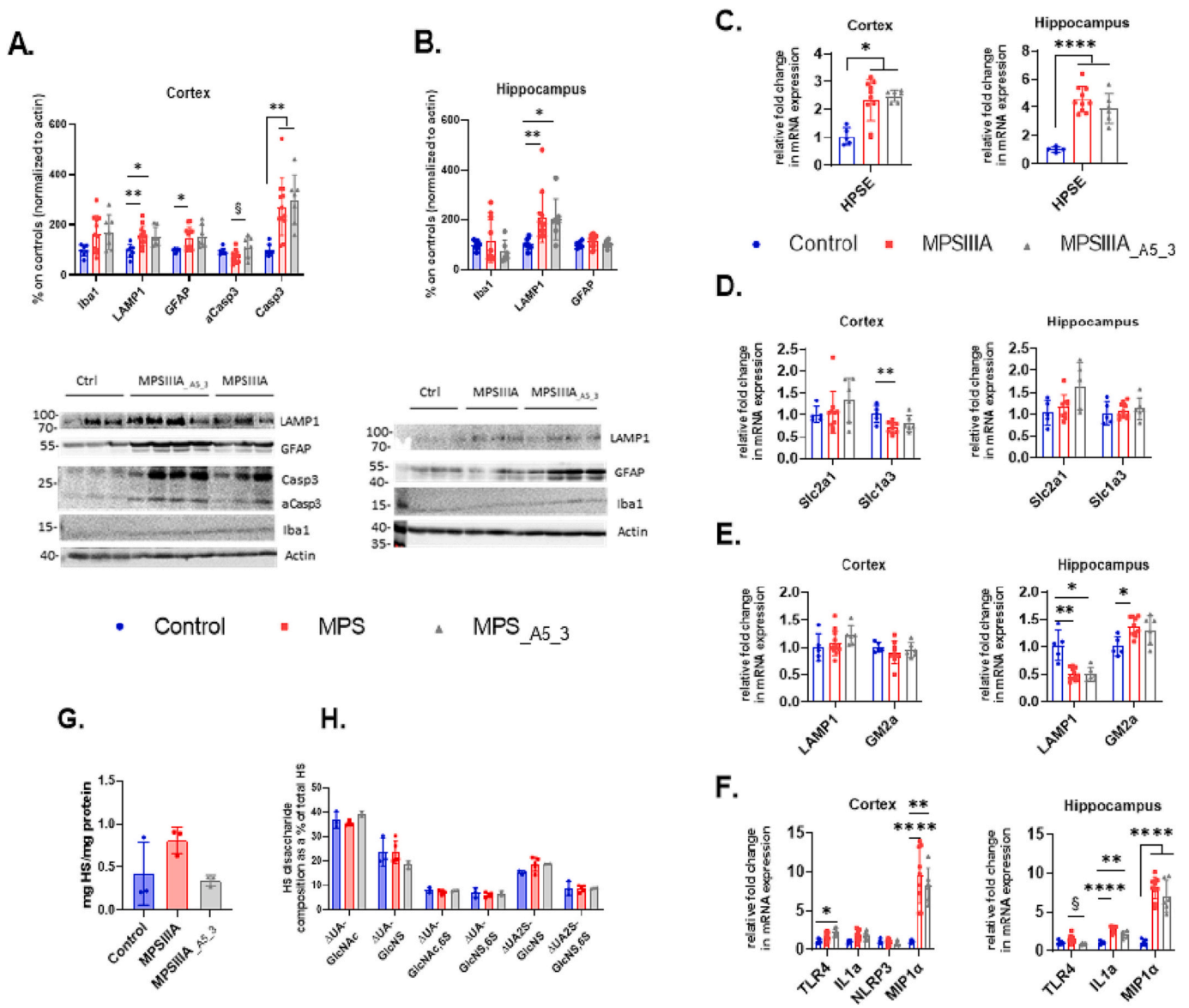

Fig. 5. Pathological phenotypes of MPSIIIA mice at 12 weeks. Protein expression in the cortex and hippocampus of control and MPSIIIA mice at 12 weeks (panels A and B). Bar graphs represents immunoblots of microglia (Iba-1), cell death (aCasp3), lysosomes (LAMP1) and astrogliosis (GFAP). Results are normalized to the control level expression (100 %). Representative immunoblots are reported below the graphs. Panels C-F: mRNA relative to the reference rps18 mRNA for heparanase (HPSE), energy metabolism (Slc2a1, Slc1a3), the lysosomal marker LAMP1 and G_{M2} activator protein (GM2A), inflammation (MIP-1α, TLR4, IL-1α) and inflammasome component NLRP3. Results are normalized to the control level expression. Panels G-H: quantification and structural characterization of HS disaccharides obtained from HS isolated from the prefrontal cortex. Significance testing was determined using one-way ANOVA or Kruskal-Wallis: * Control *vs* MPSIIIA (*$p < 0.05$, **$p < 0.01$, ***$p < 0.001$, ****$p < 0.0001$), § MPSIIIA *vs* MPSIIIA treated with A5_3, $p < 0.05$.

(Depar) in the external capsule ($p = 0.008$) and cWM ($p = 0.015$). This effect was reversed by A5_3 in the cWM. The intra-axonal volume fraction (fin) was decreased in the external capsule ($p = 0.027$) and in the motor cortex of MPSIIIA mice, while treatment was able to decrease the levels of C2 (square of the cosine of the angle between the fibers). Overall, advanced magnetic resonance techniques show damage to the microstructure integrity in myelinated tracts in MPSIIIA mice and partial restorative effects of A5_3.

3.6. Autoradiography

[^{125}I]-CLINDE autoradiography was used to quantify the expression of TSPO (18 kDa translocator protein) which is a marker of neurodegeneration increased in the presence of neuroinflammation and overexpressed in activated microglia and reactive astrocytes (Tournier et al., 2020). Although increased TSPO levels were detected in the hippocampus of MPSIIIA mice with an effect of treatment, data did not reach statistical significance (Fig. S12).

4. Discussion

In this study, we provide both *in vitro* and *in vivo* data regarding the use of marine polysaccharides with HPSE-inhibiting activity in the context of Sanfilippo syndrome. On the MPSIIIA cell line we observed limited degradation of intracellular HS upon treatment and this prompted us to investigate the possible effects of the selected compound (A5_3) in a MPSIIIA mouse model. Following an 8-week protocol of i.p. injections of A5_3 we observed some behavioral benefits and protective effects over brain metabolism, microstructure and neuroinflammation.

Inhibition of HPSE by marine polysaccharides was not as strong as

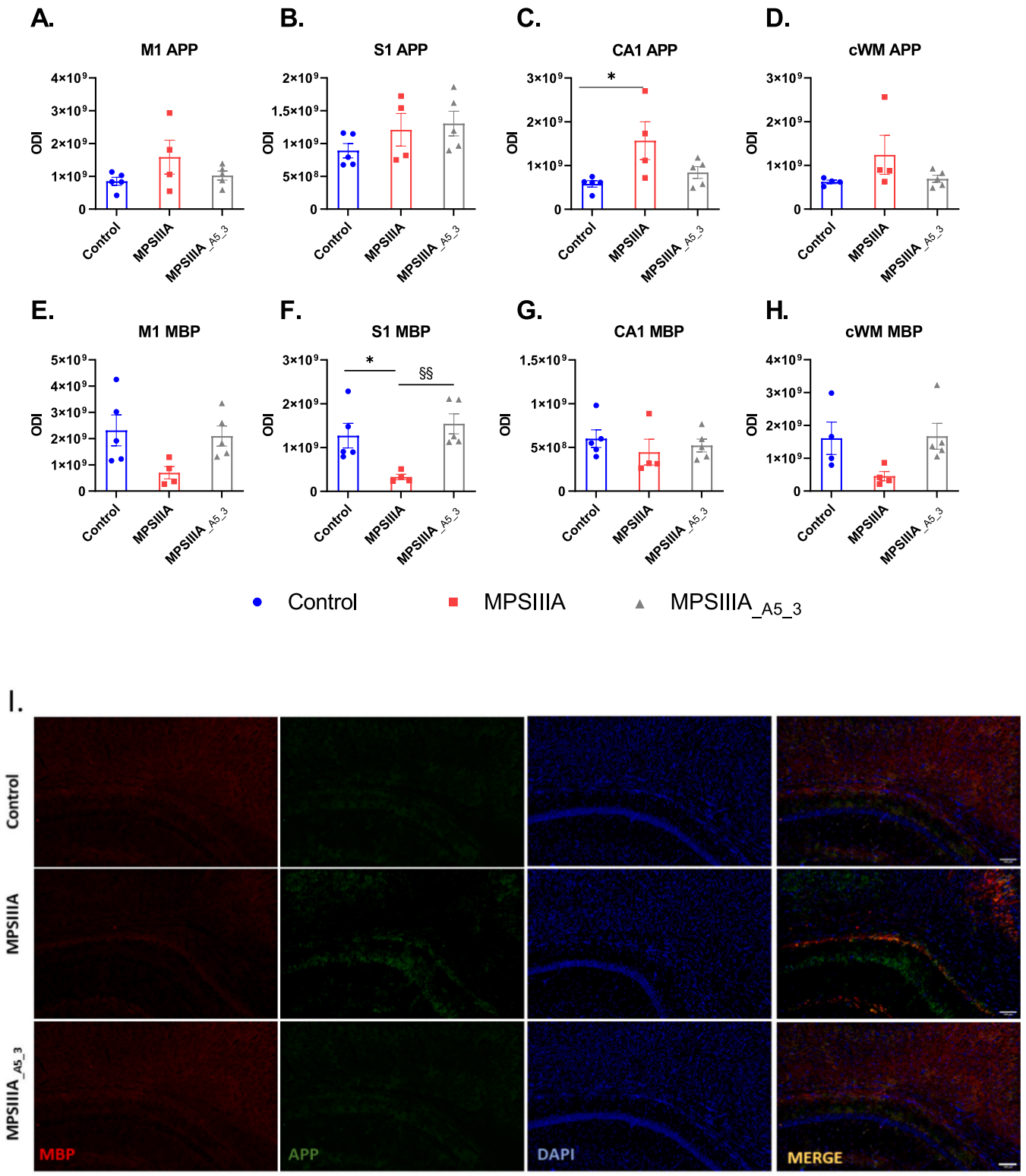

Fig. 6. Increased neurodegeneration (APP) and decreased myelination (MBP) markers in the brain of MPSIIIA mice are ameliorated upon treatment. APP (panels A-D) and MBP (panels *E*-H) were quantified in two regions of the cortex (M1 and S1), one region of the hippocampus (CA1) and the medial cingulate white matter (cWM) from 12-week-old mice and expressed as mean ± SEM. Representative images of CA1 and cWM regions are shown in panel I, respectively (APP in green, MBP in red, DAPI in blue). One-way ANOVA or Kruskal-Wallis, * Control *vs* MPSIIIA, § MPSIIIA *vs* MPSIIIA treated with A5_3, $p < 0.05$. Scale bar: 100 μm.

RO heparin (in our tests) or other more potent compounds described in literature (Hammond, Khurana, Shridhar, & Dredge, 2014).VLRO heparin was not analyzed; however, it is known that smaller RO heparin derivatives have anti-HPSE activity (Ni et al., 2016). Interestingly, all four polysaccharides tested led to reduced degradation of intracellular HS, with marine polysaccharides being slightly more efficient than heparin derivatives (Table 2). Comparable effects were observed with different concentrations of polysaccharides (10 μg/ml already showing

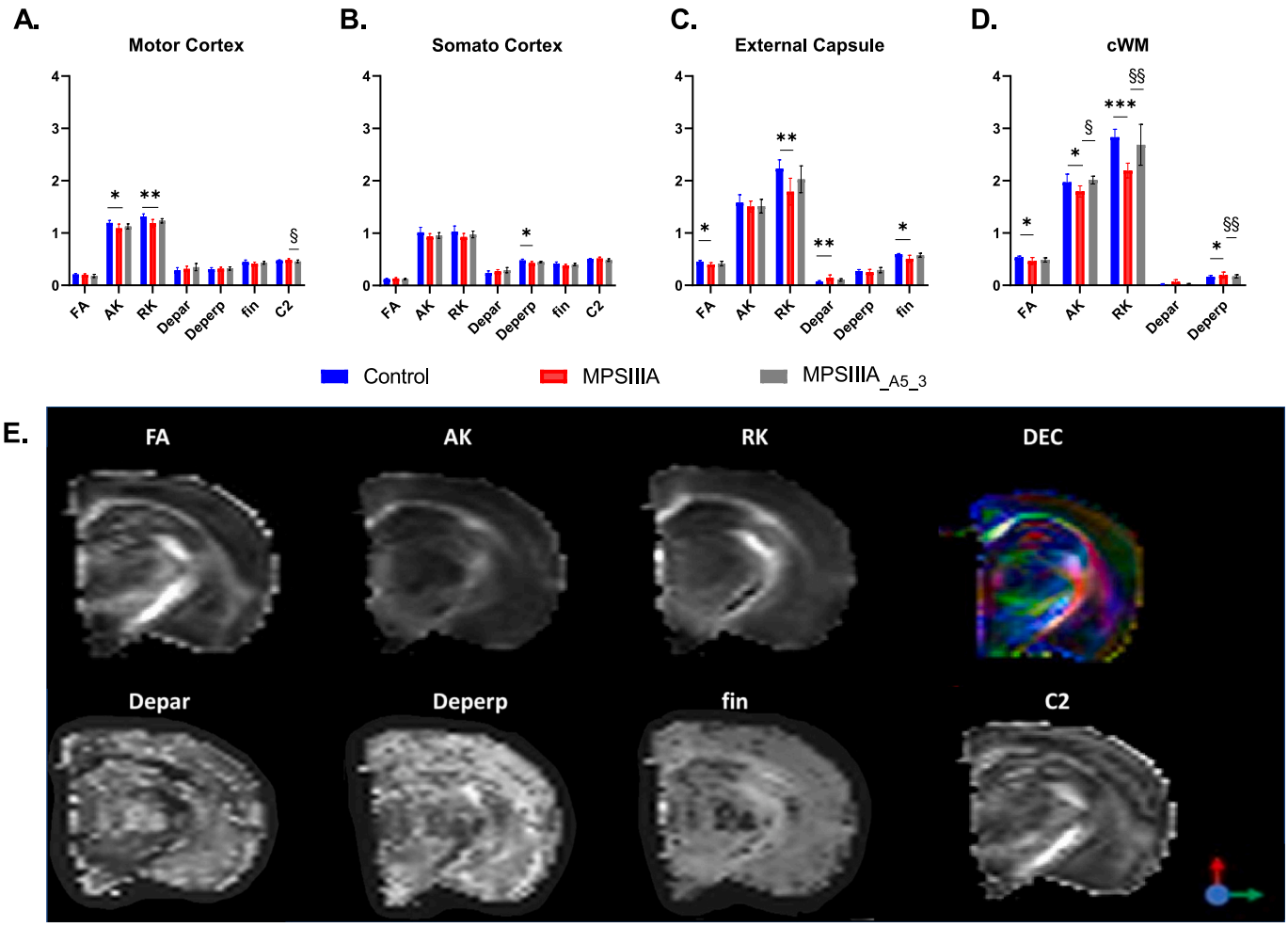

Fig. 7. *Ex vivo* Diffusion Tensor Imaging reveals damage to the brain microstructure in MPSIIIA mice with a neuroprotective effect of treatment. Panels A-D: FA (fractional anisotropy), AK (axial kurtosis), RK (radial kurtosis), Depar (diffusivity extra-axonal parallel to the fibers), Deperp (diffusivity extra-axonal perpendicular to the fibers), fin (intra-axonal volume fraction) and C2 (squared cosine of the angle between the fibers) in the somatosensory cortex, motor cortex, external capsule and medial cWM regions. Panel E: representative images of FA, AK, RK, direction encoded colour maps (DEC), Depar, Deperp, fin and C2 in the somato and motor cortices as well as external capsule and medial cWM region. Data are expressed as mean ± SD ($n = 6$) of arbitrary units except diffusivity values expressed as $\times 10^{-3}$ $mm^2.s^{-1}$. One-way ANOVA, * Control *vs* MPSIIIA, § MPSIIIA *vs* MPSIIIA treated with A5_3, ** $p < 0.001$, **** <0.0001.

activity) and independently from both the size and sulfate content (varying from 30 % for heparins to 40 % for A5_3). Notably, for *in vivo* tests targeting the CNS, the molecular weight of compounds is a major parameter to be considered. Compromised integrity of the BBB was observed in MPSIIIB mice from 3 months of age (Garbuzova-Davis et al., 2011), suggesting the possible entry of molecules between 3 and 15 kDa. However, the elevated sulfation level of the polysaccharides presented in this study increases their hydrodynamic shell, which led us to prefer compounds with lower molecular weight (VLRO and A5_3) and especially A5_3, due to its origin from a renewable source.

In vitro, we did not detect HPSE inhibitors in the intracellular fraction, thus suggesting that their mechanism of action could be the direct competition for HPSE binding on the cell surface, thereby preventing HS-proteoglycans from being internalized for degradation. Nevertheless, we did not detect decreased intracellular HS, rather a shift in its molecular weight, with less accumulation of LMW HS toxic fragments. These results are consistent with our original hypothesis that HPSE inhibition could favorably impact HS turnover. Interestingly, a trend in increased HS content in the prefrontal cortex of the MPSIIIA mouse model was observed (Fig. 5, panels G and H), similarly to (Ausseil et al., 2008; Wilkinson et al., 2012), and which was counteracted by A5_3.

To obtain an overview of the *in vivo* effects of A5_3 treatment, we combined ^{1}H-MRS analysis with protein and gene expression and behavior outputs. High field ^{1}H-MRS enabled us to investigate changes in the "neurochemical profile" of the mouse brain during development (Fig. 3) (van de Looij, Vasung, Sizonenko, & Huppi, 2014). To the best of our knowledge, ^{1}H-MRS spectroscopy and DTI have not been used previously to study MPSIIIA mice. MRS at an early stage (4 weeks of age) revealed alterations in MPSIIIA mice, highlighting early metabolic disequilibrium in the CNS and affecting in greater extent the cortex. Energy metabolism and healthy cellular function markers, such as creatine, phosphocreatine and macromolecules were reduced, which is consistent with findings from metabolomic analysis in the serum of MPSIIIA and MPSIIIB patients (Fu et al., 2017). By looking at the evolution of metabolites in the cortex from 4 to 12 weeks, their level tended to remain constant or to decrease in control mice, while in contrast, most metabolites increased with age in MPSIIIA (data not shown). As a consequence, less metabolites were altered between MPSIIIA and control mice at 12 weeks, suggesting that MPSIIIA mice might produce more metabolites over time in order to 'compensate' the initial disequilibrium in the neurochemical profile, thus impacting the neurodevelopment of animals. Also, the decreased levels of macromolecules (Mac) in the cortex and hippocampus at 4 weeks provide initial evidence of tissue and cell integrity disruption in the MPSIIIA mouse model. The reduction in glutamate and taurine indicate mitochondrial impairment, neuronal integrity loss and neurotransmission deficits (van de Looij, Dean, Gunn,

Huppi, & Sizonenko, 2015). Our data reinforce the importance of *in vivo* imaging in the early detection of brain metabolic dysfunction preceding neurodegeneration and cognitive decline. Treatment with A5_3 restored brain metabolism by normalizing the levels of some metabolites (namely Lac in the cortex) as well as Tau in the hippocampus after treatment.

The combination of techniques used for *ex vivo* brain imaging enabled the identification of white matter fiber orientation and integrity, as well as its quantitative anisotropy as surrogate markers of microstructure (Fig. 7). Particularly, DKI (diffusion kurtosis imaging) has potential sensitivity to demonstrate microstructural properties of the tissue, which has been shown to be correlated with cognitive deficits and cortical alterations (Ostergaard et al., 2014). In our study, decreased fractional anisotropy was observed– likewise found in a murine model of MPSVII (Kumar et al., 2014) and in a canine model of MPSI (Middleton et al., 2018). Also, the increase in extra-axonal diffusivity in the white matter of MPSIIIA animals is consistent with the defective myelination observed in MPSIIIB mice (Wilkinson et al., 2012) and in both MPSIIIC patients and mice (Taherzadeh et al., 2023). Such findings indicate that A5_3 treatment had an effect on preventing the white matter damage observed in MPSIIIA mice. The breakdown of myelin and inability to regenerate fully myelinated oligodendrocytes are correlated with several neurodegenerative diseases. Our data on reduced MBP and increased APP in MPSIIIA mouse cortical and subcortical areas (Fig. 6) correlate with literature data on AD patients describing significant loss of intact MBP (Zhan et al., 2014) which is mostly present at the margins of amyloid plaques where the myelin damage could be the result of toxic effects of APP over-expression (Zhan et al., 2015). Unlikely AD, the TSPO protein, which was shown to be overexpressed in activated microglia and reactive astrocytes, was not altered in our MPSIIIA mouse model.

MPSIIIA mice at 12 weeks did not present with a complete neurodegenerative profile, as we did not observe significant increase in markers associated to microglia and astrocyte activation except for GFAP and a trend for Iba-1 in the cortex. This could be linked to the early disease stage with mainly apoptosis that triggers less inflammation than necrosis. A trend towards augmented CD68 was observed in MPSIIIA animals (and further increased upon treatment), suggestive of microglial phagocytic activity and possibly resulting in increased removal of cell debris. Behavioral analysis showed a decreased pattern of activity in the Open Field test in accordance with (Lau, Crawley, Hopwood, & Hemsley, 2008; Soe et al., 2019) and improved coordination in the Beam Balance test. On the contrary, we did not observe significant impairments in memory performance in MPSIIIA animals in the Y-Maze test (Fig. S13) and described by other groups in the Morris Water Maze (Crawley et al., 2006; Parker et al., 2020). However, the cited studies used older animals compared to ours, not allowing a proper comparison. Muscular resistance was not altered in MPSIIIA mice in the Hang Wire test (Fig. S13) in disagreement with previous findings showing reduced grip strength in this model (Crawley et al., 2006). It is worth mentioning that literature data on the MPSIIIA mouse model vary considerably according to the sex and age of the animals assessed (Crawley et al., 2006; McIntyre et al., 2008). Indeed, the discrepancies we observed could be a result of the early endpoint used in this study, as the behavioral phenotype of the mouse model of MPSIIIA was described as being present from 16 weeks of age (Crawley et al., 2006).

Increased transcription of genes related to the synthesis of HPSE, as well as inflammatory cytokines and elements that mediate the inflammatory response was observed in MPSIIIA mice. HPSE also has non-enzymatic activity and is involved in the regulation of chromatin remodeling (Yang et al., 2018) and of autophagy (Shteingauz et al., 2015) and impairment of the autophagic-lysosomal pathway was described in MPSIII. Although A5_3 was shown to inhibit HPSE activity *in vitro* and to impact HS turnover in the cell line, this effect did not translate into an effect on HPSE transcription nor expression in tissue (Fig. S9). *In vivo* results did not point out a specific pathway to be investigated but suggested preservation of myelination and white matter metabolic alterations as a possible future study direction. A5_3 also inhibited the activity of SULF2 (Fig. S14). SULFs are extracellular endosulfatases, which have emerged as critical regulators of HS structure and functions, through their ability to remodel HS 6-O-sufation pattern. Although a possible interplay with HPSE has not been investigated yet, this could be highly relevant for many pathophysiological processes. Indeed, like HPSE, SULFs has been associated with tumor progression (Vives, Seffouh, & Lortat-Jacob, 2014), Alzheimer/protein aggregation diseases (Hosono-Fukao et al., 2012; Iwahashi et al., 2020) and inflammation (El Masri, Cretinon, Gout, & Vives, 2020). Further investigation is needed to assess whether the inhibitory effect of A5_3 on the SULFs could be relevant in the context of MPSIIIA. However, marine polysaccharides are able to exert pleiotropic effects similarly to heparin, therefore we cannot exclude that their mechanism of action passes through other routes than HPSE; nevertheless, our data highlight the potential of A5_3 to act on the two major enzymes involved in the post-synthesis regulation of HS.

Taken together, our results expand the characterization of the neuropathology and phenotype of the MPSIIIA mouse model, especially by MRS and DTI analyses. We provide new evidence of early brain metabolic dysfunction in MPSIIIA mice; this behavioral decline, if counteracted in its initial stages, could be at least slowed down to prevent neurodegeneration. Importantly, this study is the first to demonstrate that the repeated and prolonged administration of marine polysaccharides is a feasible approach in the context of MPSIIIA. This agrees with previous data suggesting that strategies used to reduce or alter HS accumulation might be employed for the treatment of rare diseases with minimal deleterious effects (Lamanna et al., 2012). Interestingly, it has to be noticed that the effects of A5_3 treatment on the MPSIIIA mouse model were caused by a small fraction of the bioavailable compound. A biotinylated form of A5_3 was used for a preliminary biodistribution study following a single i.p. injection. Although results need to be confirmed, they suggest that most of the drug was excreted though urine 6 h after injection in MPSIIIA mice (Fig. S15) and probably only a small fraction of the compound reached the brain. Indeed, future investigations could use a more targeted administration route to fully exploit the potential of A5_3 treatment in neurodegenerative conditions.

CRediT authorship contribution statement

Noemi Veraldi: Investigation, Data curation, Formal analysis, Project administration, Writing – original draft. **Isabelle Dentand Quadri:** Investigation. **Yohan van de Looij:** Investigation, Formal analysis. **Laura Malaguti Modernell:** Investigation, Formal analysis. **Corinne Sinquin:** Investigation. **Agata Zykwinska:** Writing – review & editing. **Benjamin B. Tournier:** Investigation. **Fabien Dalonneau:** Investigation. **Honglian Li:** Investigation. **Jin-Ping Li:** Resources, Writing – review & editing. **Romain Vives:** Resources, Writing – review & editing. **Sylvia Colliec-Jouault:** Conceptualization, Resources, Writing – review & editing. **Ariane de Agostini:** Conceptualization, Supervision, Funding acquisition. **Eduardo Farias Sanches:** Investigation, Data curation, Formal analysis, Writing – review & editing. **Stéphane V. Sizonenko:** Resources, Supervision, Funding acquisition, Writing – review & editing.

Declaration of competing interest

The authors declare that they have no known competing financial interests or personal relationships that could have appeared to influence the work reported in this paper.

Data availability

Data will be made available on request.

Acknowledgements

Research was supported by the Fondation Sanfilippo Suisse. We thank Dr. Analina Hausin, Dr. Mario Lepore and Dr. Stefanita Mitrea from the CIBM in Lausanne for their precious help with animals. We thank Annamaria Naggi from Ronzoni Institute for providing heparin derivatives and Dr. Edwin Yates of Liverpool University for critical reading. All authors have read the journal's policy on disclosure of potential conflicts of interest and declare no conflict of interest. All authors have read and approved the final version of the manuscript as submitted.

Appendix A. Supplementary data

Supplementary data to this article can be found online at https://doi.org/10.1016/j.carbpol.2023.121214.

References

Alekseeva, A., Casu, B., Cassinelli, G., Guerrini, M., Torri, G., & Naggi, A. (2014). Structural features of glycol-split low-molecular-weight heparins and their heparin lyase generated fragments. *Analytical and Bioanalytical Chemistry, 406*(1), 249–265. https://doi.org/10.1007/s00216-013-7446-4

Alexopoulou, A. N., Multhaupt, H. A., & Couchman, J. R. (2007). Syndecans in wound healing, inflammation and vascular biology. *The International Journal of Biochemistry & Cell Biology, 39*(3), 505–528. https://doi.org/10.1016/j.biocel.2006.10.014

Ausseil, J., Desmaris, N., Bigou, S., Attali, R., Corbineau, S., Vitry, S., … Heard, J. M. (2008). Early neurodegeneration progresses independently of microglial activation by heparan sulfate in the brain of mucopolysaccharidosis IIIB mice. *PLoS One, 3*(5), Article e2296. https://doi.org/10.1371/journal.pone.0002296

Bailey, K. R., & Crawley, J. N. (2009). Anxiety-related behaviors in mice. In nd & J. J. Buccafusco (Eds.), *methods of behavior analysis in neuroscience*. https://www.ncbi.nlm.nih.gov/pubmed/21204329.

Beard, H., Hassiotis, S., Gai, W. P., Parkinson-Lawrence, E., Hopwood, J. J., & Hemsley, K. M. (2017). Axonal dystrophy in the brain of mice with Sanfilippo syndrome. *Experimental Neurology, 295*, 243–255. https://doi.org/10.1016/j.expneurol.2017.06.010

Bergamaschini, L., Rossi, E., Storini, C., Pizzimenti, S., Distaso, M., Perego, C., … De Simoni, M. G. (2004). Peripheral treatment with enoxaparin, a low molecular weight heparin, reduces plaques and beta-amyloid accumulation in a mouse model of Alzheimer's disease. *The Journal of Neuroscience, 24*(17), 4181–4186. https://doi.org/10.1523/JNEUROSCI.0550-04.2004

Bertini, S., Bisio, A., Torri, G., Bensi, D., & Terbojevich, M. (2005). Molecular weight determination of heparin and dermatan sulfate by size exclusion chromatography with a triple detector array. *Biomacromolecules, 6*(1), 168–173. https://doi.org/10.1021/bm049693s

Bhaumik, M., Muller, V. J., Rozaklis, T., Johnson, L., Dobrenis, K., Bhattacharyya, R., … Stanley, P. (1999). A mouse model for mucopolysaccharidosis type III a (Sanfilippo syndrome). *Glycobiology, 9*(12), 1389–1396. https://doi.org/10.1093/glycob/9.12.1389

Bruyere, J., Roy, E., Ausseil, J., Lemonnier, T., Teyre, G., Bohl, D., … Vitry, S. (2015). Heparan sulfate saccharides modify focal adhesions: Implication in mucopolysaccharidosis neuropathophysiology. *Journal of Molecular Biology, 427*(4), 775–791. https://doi.org/10.1016/j.jmb.2014.09.012

Chopin, N., Sinquin, C., Ratiskol, J., Zykwinska, A., Weiss, P., Cerantola, S., … Colliec-Jouault, S. (2015). A direct Sulfation process of a marine polysaccharide in ionic liquid. *BioMed Research International, 2015*, Article 508656. https://doi.org/10.1155/2015/508656

Clarke, L. A. (2008). The mucopolysaccharidoses: a success of molecular medicine. *Expert Reviews in Molecular Medicine, 10*, Article e1. https://doi.org/10.1017/S1462399408000550

Colliec Jouault, S., Chevolot, L., Helley, D., Ratiskol, J., Bros, A., Sinquin, C., … Fischer, A. M. (2001). Characterization, chemical modifications and in vitro anticoagulant properties of an exopolysaccharide produced by Alteromonas infernus. *Biochimica et Biophysica Acta, 1528*(2–3), 141–151. https://doi.org/10.1016/s0304-4165(01)00185-4

Colliec-Jouault, S., Esposito, F., Ledru, H., Sinquin, C., Marchand, L., Fillaudeau, A., Routier, S., Buron, F., Lopin-Bon, C., Cuenot, S., Bedinini, E., & Zykwinska, A. (2023). Glycosaminoglycan mimetics obtained by microwave-assisted sulfation of marine bacterium sourced infernan exopolysaccharide. *Biomacromolecules, 24*, 462–470.

Conrad, H. E., & Guo, Y. (1992). Structural analysis of periodate-oxidized heparin. In D. A. Lane, I. Björk, & U. Lindahl (Eds.) (ed.,, *Vol. 313. Advances in experimental medicine and biology* (pp. 31–36). New York: Plenum Press.

Crawley, A. C., Gliddon, B. L., Auclair, D., Brodie, S. L., Hirte, C., King, B. M., … Hopwood, J. J. (2006). Characterization of a C57BL/6 congenic mouse strain of mucopolysaccharidosis type IIIA. *Brain Research, 1104*(1), 1–17. https://doi.org/10.1016/j.brainres.2006.05.079

El Masri, R., Cretinon, Y., Gout, E., & Vives, R. R. (2020). HS and inflammation: A potential playground for the Sulfs? *Frontiers in Immunology, 11*, 570. https://doi.org/10.3389/fimmu.2020.00570

Esposito, F., Vessella, G., Sinquin, C., Traboni, S., Iadonisi, A., Colliec-Jouault, S., … Bedini, E. (2022). Glycosaminoglycan-like sulfated polysaccharides from Vibrio diabolicus bacterium: Semi-synthesis and characterization. *Carbohydrate Polymers, 283*, Article 119054. https://doi.org/10.1016/j.carbpol.2021.119054

Fu, H., Meadows, A. S., Pineda, R. J., Mohney, R. P., Stirdivant, S., & McCarty, D. M. (2017). Serum global metabolomics profiling reveals profound metabolic impairments in patients with MPS IIIA and MPS IIIB. *Metabolic Brain Disease, 32*(5), 1403–1415. https://doi.org/10.1007/s11011-017-0009-1

Galli, M., Chatterjee, M., Grasso, M., Specchia, G., Magen, H., Einsele, H., … Nagler, A. (2018). Phase I study of the heparanase inhibitor roneparstat: An innovative approach for ultiple myeloma therapy. *Haematologica, 103*(10), e469–e472. https://doi.org/10.3324/haematol.2017.182865

Garbuzova-Davis, S., Louis, M. K., Haller, E. M., Derasari, H. M., Rawls, A. E., & Sanberg, P. R. (2011). Blood-brain barrier impairment in an animal model of MPS III B. *PLoS One, 6*(3), Article e16601. https://doi.org/10.1371/journal.pone.0016601

Gitay-Goren, H., Soker, S., Vlodavsky, I., & Neufeld, G. (1992). The binding of vascular endothelial growth factor to its receptors is dependent on cell surface-associated heparin-like molecules. *The Journal of Biological Chemistry, 267*(9), 6093–6098. https://www.ncbi.nlm.nih.gov/pubmed/1556117.

Gleitz, H. F., O'Leary, C., Holley, R. J., & Bigger, B. W. (2017). Identification of age-dependent motor and neuropsychological behavioural abnormalities in a mouse model of Mucopolysaccharidosis type II. *PLoS One, 12*(2), Article e0172435. https://doi.org/10.1371/journal.pone.0172435

Gruetter, R., & Tkac, I. (2000). Field mapping without reference scan using asymmetric echo-planar techniques. *Magnetic Resonance in Medicine, 43*(2), 319–323. https://doi.org/10.1002/(sici)1522-2594(200002)43:2<319::aid-mrm22>3.0.co;2-1

Guo, N., DeAngelis, V., Zhu, C., Schuchman, E. H., & Simonaro, C. M. (2019). Pentosan Polysulfate treatment of Mucopolysaccharidosis type IIIA mice. *JIMD Rep, 43*, 37–52. https://doi.org/10.1007/8904_2018_96

Hammond, E., Khurana, A., Shridhar, V., & Dredge, K. (2014). The role of Heparanase and sulfatases in the modification of Heparan sulfate proteoglycans within the tumor microenvironment and opportunities for novel Cancer therapeutics. *Frontiers in Oncology, 4*, 195. https://doi.org/10.3389/fonc.2014.00195

Hasegawa, Y., Hayashi, K., Takemoto, Y., Cheng, C., Takane, K., Lin, B., … Kim-Mitsuyama, S. (2017). DPP-4 inhibition with linagliptin ameliorates the progression of premature aging in klotho−/− mice. *Cardiovascular Diabetology, 16*(1), 154. https://doi.org/10.1186/s12933-017-0639-y

Henriet, E., Jager, S., Tran, C., Bastien, P., Michelet, J. F., Minondo, A. M., … Vives, R. R. (2017). A jasmonic acid derivative improves skin healing and induces changes in proteoglycan expression and glycosaminoglycan structure. *Biochimica et Biophysica Acta - General Subjects, 1861*(9), 2250–2260. https://doi.org/10.1016/j.bbagen.2017.06.006

Heymann, D., Ruiz-Velasco, C., Chesneau, J., Ratiskol, J., Sinquin, C., & Colliec-Jouault, S. (2016). Anti-metastatic properties of a marine bacterial exopolysaccharide-based derivative designed to mimic Glycosaminoglycans. *Molecules, 21*(3), 309. https://doi.org/10.3390/molecules21030309

Holley, R. J., Ellison, S. M., Fil, D., O'Leary, C., McDermott, J., Senthivel, N., … Bigger, B. W. (2018). Macrophage enzyme and reduced inflammation drive brain correction of mucopolysaccharidosis IIIB by stem cell gene therapy. *Brain, 141*(1), 99–116. https://doi.org/10.1093/brain/awx311

Hopwood, J. J. (1989). Enzymes that degrade heparin and heparan sulphate. In D. W. a. L. Lane, U. (Ed.), *Heparin: Chemical and biological properties, clinical applications* (Edward Arnold, London ed., pp. 191).

Hosono-Fukao, T., Ohtake-Niimi, S., Hoshino, H., Britschgi, M., Akatsu, H., Hossain, M. M., … Uchimura, K. (2012). Heparan sulfate subdomains that are degraded by Sulf accumulate in cerebral amyloid ss plaques of Alzheimer's disease: Evidence from mouse models and patients. *The American Journal of Pathology, 180*(5), 2056–2067. https://doi.org/10.1016/j.ajpath.2012.01.015

Iwahashi, N., Ikezaki, M., Nishikawa, T., Namba, N., Ohgita, T., Saito, H., … Nishitsuji, K. (2020). Sulfated glycosaminoglycans mediate prion-like behavior of p53 aggregates. *Proceedings of the National Academy of Sciences of the United States of America, 117*(52), 33225–33234. https://doi.org/10.1073/pnas.2009931117

Jespersen, S. N., Olesen, J. L., Hansen, B., & Shemesh, N. (2018). Diffusion time dependence of microstructural parameters in fixed spinal cord. *Neuroimage, 182*, 329–342. https://doi.org/10.1016/j.neuroimage.2017.08.039

Kumar, M., Nasrallah, I. M., Kim, S., Ittyerah, R., Pickup, S., Li, J., … Poptani, H. (2014). High-resolution magnetic resonance microscopy and diffusion tensor imaging to assess brain structural abnormalities in the murine mucopolysaccharidosis VII model. *Journal of Neuropathology and Experimental Neurology, 73*(1), 39–49. https://doi.org/10.1097/NEN.0000000000000023

Lamanna, W. C., Lawrence, R., Sarrazin, S., Lameda-Diaz, C., Gordts, P. L., Moremen, K. W., & Esko, J. D. (2012). A genetic model of substrate reduction therapy for mucopolysaccharidosis. *The Journal of Biological Chemistry, 287*(43), 36283–36290. https://doi.org/10.1074/jbc.M112.403360

Langford-Smith, A., Langford-Smith, K. J., Jones, S. A., Wynn, R. F., Wraith, J. E., Wilkinson, F. L., & Bigger, B. W. (2011). Female mucopolysaccharidosis IIIA mice exhibit hyperactivity and a reduced sense of danger in the open field test. *PLoS One, 6*(10), Article e25717. https://doi.org/10.1371/journal.pone.0025717

Lau, A. A., Crawley, A. C., Hopwood, J. J., & Hemsley, K. M. (2008). Open field locomotor activity and anxiety-related behaviors in mucopolysaccharidosis type IIIA mice. *Behavioural Brain Research, 191*(1), 130–136. https://doi.org/10.1016/j.bbr.2008.03.024

van de Looij, Y., Chatagner, A., Huppi, P. S., Gruetter, R., & Sizonenko, S. V. (2011). Longitudinal MR assessment of hypoxic ischemic injury in the immature rat brain. *Magnetic Resonance in Medicine, 65*(2), 305–312. https://doi.org/10.1002/mrm.22617

van de Looij, Y., Dean, J. M., Gunn, A. J., Huppi, P. S., & Sizonenko, S. V. (2015). Advanced magnetic resonance spectroscopy and imaging techniques applied to brain development and animal models of perinatal injury. *International Journal of Developmental Neuroscience, 45*, 29–38. https://doi.org/10.1016/j.ijdevneu.2015.03.009

van de Looij, Y., Vasung, L., Sizonenko, S. V., & Huppi, P. S. (2014). MRI of animal models of developmental disorders and translation to human imaging. *Current Opinion in Neurology, 27*(2), 157–167. https://doi.org/10.1097/WCO.0000000000000066

Malinowska, M., Wilkinson, F. L., Langford-Smith, K. J., Langford-Smith, A., Brown, J. R., Crawford, B. E., … Bigger, B. W. (2010). Genistein improves neuropathology and corrects behaviour in a mouse model of neurodegenerative metabolic disease. *PLoS One, 5*(12), Article e14192. https://doi.org/10.1371/journal.pone.0014192

Martins, C., Hulkova, H., Dridi, L., Dormoy-Raclet, V., Grigoryeva, L., Choi, Y., … Pshezhetsky, A. V. (2015). Neuroinflammation, mitochondrial defects and neurodegeneration in mucopolysaccharidosis III type C mouse model. *Brain, 138*(Pt 2), 336–355. https://doi.org/10.1093/brain/awu355

McIntyre, C., Derrick Roberts, A. L., Ranieri, E., Clements, P. R., Byers, S., & Anson, D. S. (2008). Lentiviral-mediated gene therapy for murine mucopolysaccharidosis type IIIA. *Molecular Genetics and Metabolism, 93*(4), 411–418. https://doi.org/10.1016/j.ymgme.2007.11.008

Middleton, D. M., Li, J. Y., Chen, S. D., White, L. E., Dickson, P., Ellinwood, N. M., & Provenzale, J. M. (2018). Diffusion tensor imaging findings suggestive of white matter alterations in a canine model of mucopolysaccharidosis type I. *The Neuroradiology Journal, 31*(1), 90–94. https://doi.org/10.1177/1971400917715792

Mlynarik, V., Gambarota, G., Frenkel, H., & Gruetter, R. (2006). Localized short-echo-time proton MR spectroscopy with full signal-intensity acquisition. *Magnetic Resonance in Medicine, 56*(5), 965–970. https://doi.org/10.1002/mrm.21043

Mulloy, B., Gee, C., Wheeler, S. F., Wait, R., Gray, E., & Barrowcliffe, T. W. (1997). Molecular weight measurements of low molecular weight heparins by gel permeation chromatography. *Thrombosis and Haemostasis, 77*(4), 668–674. https://www.ncbi.nlm.nih.gov/pubmed/9134640.

Ni, M., Elli, S., Naggi, A., Guerrini, M., Torri, G., & Petitou, M. (2016). Investigating glycol-Split-heparin-derived inhibitors of Heparanase: A study of synthetic Trisaccharides. *Molecules, 21*(11). https://doi.org/10.3390/molecules21111602

Ostergaard, L., Engedal, T. S., Aamand, R., Mikkelsen, R., Iversen, N. K., Anzabi, M., … Rasmussen, M. (2014). Capillary transit time heterogeneity and flow-metabolism coupling after traumatic brain injury. *Journal of Cerebral Blood Flow and Metabolism, 34*(10), 1585–1598. https://doi.org/10.1038/jcbfm.2014.131

Parker, H., Ellison, S. M., Holley, R. J., O'Leary, C., Liao, A., Asadi, J., … Bigger, B. W. (2020). Haematopoietic stem cell gene therapy with IL-1Ra rescues cognitive loss in mucopolysaccharidosis IIIA. *EMBO Molecular Medicine, 12*(3), Article e11185. https://doi.org/10.15252/emmm.201911185

Pearse, Y., & Iacovino, M. (2020). A cure for Sanfilippo syndrome? A summary of current therapeutic approaches and their promise. *Med Res Arch, 8*(2). https://doi.org/10.18103/mra.v8i2.2045

Phillips, H. J. (1973). Dye exclusion test for cell viability. In P. K. a. P. Krude, M. K. Jr. (Ed.), *Tissue culture methods and applications* (pp. 406–408). New Yors: Academic Press.

Provencher, S. W. (1993). Estimation of metabolite concentrations from localized in vivo proton NMR spectra. *Magnetic Resonance in Medicine, 30*(6), 672–679. https://doi.org/10.1002/mrm.1910300604

Prut, L., & Belzung, C. (2003). The open field as a paradigm to measure the effects of drugs on anxiety-like behaviors: a review. *European Journal of Pharmacology, 463*(1–3), 3–33. https://doi.org/10.1016/s0014-2999(03)01272-x

Roger, O., Kervarec, N., Ratiskol, J., Colliec-Jouault, S., & Chevolot, L. (2004). Structural studies of the main exopolysaccharide produced by the deep-sea bacterium Alteromonas infernus. *Carbohydrate Research, 339*, 2371–2380.

Rougeaux, H., Kervarec, N., Pichon, R., & Guezennec, J. (1999). Structure of the exopolysaccharide of Vibrio diabolicus isolated from a deep-sea hydrothermal vent. *Carbohydrate Research, 322*(1–2), 40–45. https://doi.org/10.1016/s0008-6215(99)00214-1

Sanches, E. F., Carvalho, A. S., van de Looij, Y., Toulotte, A., Wyse, A. T., Netto, C. A., & Sizonenko, S. V. (2021). Experimental cerebral palsy causes microstructural brain damage in areas associated to motor deficits but no spatial memory impairments in the developing rat. *Brain Research, 1761*, Article 147389. https://doi.org/10.1016/j.brainres.2021.147389

Seffouh, A., El Masri, R., Makshakova, O., Gout, E., Hassoun, Z. E. O., Andrieu, J. P., … Vives, R. R. (2019). Expression and purification of recombinant extracellular sulfatase HSulf-2 allows deciphering of enzyme sub-domain coordinated role for the binding and 6-O-desulfation of heparan sulfate. *Cellular and Molecular Life Sciences, 76*(9), 1807–1819. https://doi.org/10.1007/s00018-019-03027-2

Senni, K., Gueniche, F., Changotade, S., Septier, D., Sinquin, C., Ratiskol, J., … Colliec-Jouault, S. (2013). Unusual glycosaminoglycans from a deep sea hydrothermal bacterium improve fibrillar collagen structuring and fibroblast activities in engineered connective tissues. *Marine Drugs, 11*(4), 1351–1369. https://doi.org/10.3390/md11041351

Shteingauz, A., Boyango, I., Naroditsky, I., Hammond, E., Gruber, M., Doweck, I., … Vlodavsky, I. (2015). Heparanase enhances tumor growth and Chemoresistance by promoting autophagy. *Cancer Research, 75*(18), 3946–3957. https://doi.org/10.1158/0008-5472.CAN-15-0037

Soe, K., Beard, H., Neumann, D., Trim, P. J., Duplock, S., Snel, M. F., … Hemsley, K. M. (2019). Early disease course is unaltered in mucopolysaccharidosis type IIIA (MPS IIIA) mice lacking α-synuclein. *Neuropathology and Applied Neurobiology, 45*(7), 715–731. https://doi.org/10.1111/nan.12548

Taherzadeh, M. Z. E., Londono, I., Song, S.-K., Wang, S., Cooper, J. D., Kennedy, T. E., … Pshezhetsky, A. V. (2023). Severe central nervous system demyelination in Sanfilippo disease. *BiorXiv.*. https://doi.org/10.1101/2023.04.12.536631

Tournier, B. B., Tsartsalis, S., Ceyzeriat, K., Fraser, B. H., Gregoire, M. C., Kovari, E., & Millet, P. (2020). Astrocytic TSPO upregulation appears before microglial TSPO in Alzheimer's disease. *Journal of Alzheimer's Disease, 77*(3), 1043–1056. https://doi.org/10.3233/JAD-200136

Tournier, B. B., Tsartsalis, S., Ceyzeriat, K., Medina, Z., Fraser, B. H., Gregoire, M. C., … Millet, P. (2020). Fluorescence-activated cell sorting to reveal the cell origin of radioligand binding. *Journal of Cerebral Blood Flow and Metabolism, 40*(6), 1242–1255. https://doi.org/10.1177/0271678X19860408

Trudel, S., Trecherel, E., Gomila, C., Peltier, M., Aubignat, M., Gubler, B., … Ausseil, J. (2015). Oxidative stress is independent of inflammation in the neurodegenerative Sanfilippo syndrome type B. *Journal of Neuroscience Research, 93*(3), 424–432. https://doi.org/10.1002/jnr.23497

Veraldi, N., Dentand Quadri, I., & de Agostini, A. (2021). Characterization of a spontaneous cell line from primary mouse fibroblasts as a model to study Sanfilippo syndrome. *The International Journal of Biochemistry & Cell Biology, 142*, Article 106119. https://doi.org/10.1016/j.biocel.2021.106119

Vives, R. R., Seffouh, A., & Lortat-Jacob, H. (2014). Post-synthetic regulation of HS structure: The yin and Yang of the Sulfs in Cancer. *Frontiers in Oncology, 3*, 331. https://doi.org/10.3389/fonc.2013.00331

Vlodavsky, I., Eldor, A., Haimovitz-Friedman, A., Matzner, Y., Ishai-Michaeli, R., Lider, O., … Fuks, Z. (1992). Expression of heparanase by platelets and circulating cells of the immune system: Possible involvement in diapedesis and extravasation. *Invasion & Metastasis, 12*(2), 112–127. https://www.ncbi.nlm.nih.gov/pubmed/1399400.

Wilkinson, F. L., Holley, R. J., Langford-Smith, K. J., Badrinath, S., Liao, A., Langford-Smith, A., … Bigger, B. W. (2012). Neuropathology in mouse models of mucopolysaccharidosis type I. *IIIA and IIIB. PLoS One, 7*(4), Article e35787. https://doi.org/10.1371/journal.pone.0035787

Wolf, A., Bauer, B., Abner, E. L., Ashkenazy-Frolinger, T., & Hartz, A. M. (2016). A comprehensive behavioral test battery to assess learning and memory in 129S6/Tg2576 mice. *PLoS One, 11*(1), Article e0147733. https://doi.org/10.1371/journal.pone.0147733

Yang, S., Liao, Y., Zhao, Q., Xie, Y., Zheng, A., & Wan, H. (2018). Heparanase is a critical regulator of mitotic spindles required for maintaining chromosome stability. *DNA and Cell Biology, 37*(4), 291–297. https://doi.org/10.1089/dna.2017.3990

Zak, B. M., Crawford, B. E., & Esko, J. D. (2002). Hereditary multiple exostoses and heparan sulfate polymerization. *Biochimica et Biophysica Acta, 1573*(3), 346–355. https://doi.org/10.1016/s0304-4165(02)00402-6

Zcharia, E., Metzger, S., Chajek-Shaul, T., Aingorn, H., Elkin, M., Friedmann, Y., … Vlodavsky, I. (2004). Transgenic expression of mammalian heparanase uncovers physiological functions of heparan sulfate in tissue morphogenesis, vascularization, and feeding behavior. *The FASEB Journal, 18*(2), 252–263. https://doi.org/10.1096/fj.03-0572com

Zhan, X., Jickling, G. C., Ander, B. P., Liu, D., Stamova, B., Cox, C., … Sharp, F. R. (2014). Myelin injury and degraded myelin vesicles in Alzheimer's disease. *Current Alzheimer Research, 11*(3), 232–238. https://doi.org/10.2174/1567205011666140131120922

Zhan, X., Jickling, G. C., Ander, B. P., Stamova, B., Liu, D., Kao, P. F., … Sharp, F. R. (2015). Myelin basic protein associates with AbetaPP, Abeta1-42, and amyloid plaques in cortex of Alzheimer's disease brain. *Journal of Alzheimer's Disease, 44*(4), 1213–1229. https://doi.org/10.3233/JAD-142013

Zhang, G. L., Zhang, X., Wang, X. M., & Li, J. P. (2014). Towards understanding the roles of heparan sulfate proteoglycans in Alzheimer's disease. *BioMed Research International, 2014*, Article 516028. https://doi.org/10.1155/2014/516028

Zykwinska, A., Marchand, L., Bonnetot, S., Sinquin, C., Colliec-Jouault, S., & Delbarre-Ladrat, C. (2019). Deep-sea hydrothermal vent Bacteria as a source of glycosaminoglycan-mimetic exopolysaccharides. *Molecules, 24*(9). https://doi.org/10.3390/molecules24091703